

Finding large counterexamples by selectively exploring the Pachner graph

Benjamin A. Burton
 The University of Queensland
 bab@maths.uq.edu.au

Alexander He
 The University of Queensland
 a.he@uqconnect.edu.au

March 14, 2023

Abstract

We often rely on censuses of triangulations to guide our intuition in 3-manifold topology. However, this can lead to misplaced faith in conjectures if the smallest counterexamples are too large to appear in our census. Since the number of triangulations increases super-exponentially with size, there is no way to expand a census beyond relatively small triangulations—the current census only goes up to 10 tetrahedra. Here, we show that it is feasible to search for large and hard-to-find counterexamples by using heuristics to *selectively* (rather than exhaustively) enumerate triangulations. We use this idea to find counterexamples to three conjectures which ask, for certain 3-manifolds, whether one-vertex triangulations always have a “distinctive” edge that would allow us to recognise the 3-manifold.

Keywords Computational topology, 3-manifolds, Triangulations, Counterexamples, Heuristics, Implementation, Pachner moves, Bistellar flips

Acknowledgements We thank the referees for their helpful comments. The second author was supported by an Australian Government Research Training Program Scholarship.

1 Introduction

There is no shortage of conjectures in computational geometry and topology that are true in small cases, but which turn out to be false in general due to the existence of a relatively large counterexample. Perhaps the most notable example of this is the *Hirsch conjecture*, which posited that in a d -dimensional polytope with n facets, any two vertices can be connected by a path of at most $n - d$ edges. It is known that the Hirsch conjecture is true when the dimension is small (specifically, when $d \leq 3$ [22]), as well as when the number of facets is small (specifically, when $n \leq d + 6$ [2]). However, these small cases are not indicative of the general behaviour: Santos showed that there is a 43-dimensional counterexample with 86 facets [34].

For an example from computational 3-manifold topology, consider the Seifert fibre spaces (see section 2.6 for a definition of these 3-manifolds). There are 302 Seifert fibre spaces that can be triangulated with no more than 7 tetrahedra; for all of these, at least one **minimal triangulation** (triangulation with the smallest possible number of tetrahedra) uses a standard prism-and-layering construction. This pattern does not persist: there is a Seifert fibre space whose unique (8-tetrahedron) minimal triangulation is given by the isomorphism signature `iLLLPQcbcggffghhhtsmhgosof` (the software package **Regina** [9] can convert this string back into a triangulation), and this triangulation is instead constructed from a gadget (called the *brick* B_5) that was first identified in Martelli and Petronio’s census of minimal triangulations up to 9 tetrahedra [25]; although the first author [4] and Matveev [27] have since extended the census, no other gadgets like this have been found.

Our main goal in this paper is to present a technique for finding large counterexamples in a similar setting to the one just mentioned. The difference is that instead of only studying properties of minimal triangulations, we consider arbitrary one-vertex triangulations. The practical motivation for this is

that one-vertex triangulations are easy to obtain, whereas it is generally difficult to know for sure whether a particular triangulation is minimal.

In our setting, the most obvious source of counterexamples would be a census of all possible triangulations up to a given number of tetrahedra. However, this only captures small counterexamples because the number of triangulations increases super-exponentially as we increase the number of tetrahedra; to date, the census of all possible closed 3-manifold triangulations only goes up to 10 tetrahedra, and this already includes over 2 billion triangulations, constituting over 63 GB of data [4].

How can we find a counterexample that is too large to appear in our census? We showcase a method of *selectively* (rather than exhaustively) enumerating triangulations, which allows us to find large counterexamples to three related conjectures posed by Saul Schleimer at the 2022 Dagstuhl workshop on *Computation and Reconfiguration in Low-Dimensional Topological Spaces*.

1.1 The conjectures

Each of the conjectures concerns properties of edges of one-vertex triangulations. Since our triangulations only have one vertex, each edge realises an embedded closed curve, so we can ask whether such an edge is embedded in an interesting or useful way.

For instance, recall that a **lens space** is a 3-manifold given by gluing together two solid tori. One way to recognise a lens space is to find a **core curve**: an embedded closed curve γ such that the complement of a regular neighbourhood of γ is a solid torus. We can ask whether one-vertex triangulations of lens spaces always contain a **core edge** (i.e., an edge that realises a core curve):

Conjecture 1. *Every one-vertex triangulation of a lens space has a core edge.*

Since solid torus recognition can be solved efficiently in practice [11, 6], proving Conjecture 1 would have provided a new and relatively efficient method for recognising lens spaces. Lens space recognition can also be used to determine whether a 3-manifold is **elliptic** (i.e., admits spherical geometry). Indeed, Lackenby and Schleimer [23] recently showed that recognising elliptic manifolds is in NP; their proof relies on the following result, which can be viewed as a variant of Conjecture 1:

Theorem ([23], Theorem 9.4). *Let \mathcal{M} be a lens space that is neither \mathbb{RP}^3 nor a prism manifold¹, and let \mathcal{T} be any triangulation of \mathcal{M} . Then the 86th iterated barycentric subdivision of \mathcal{T} contains a sequence of edges that forms a core curve.*

The other two conjectures have similar motivations: if every one-vertex triangulation of a particular type of 3-manifold contains an edge with a distinctive property, then we can use such an edge to recognise the 3-manifold.

For the second conjecture, consider a knot K in the 3-sphere. The **tunnel number** of K is the smallest number of arcs that need to be added to K so that the complement becomes a handlebody; by construction, this is a knot invariant. The three knots shown in Figure 1 are all examples of knots with tunnel number equal to one.

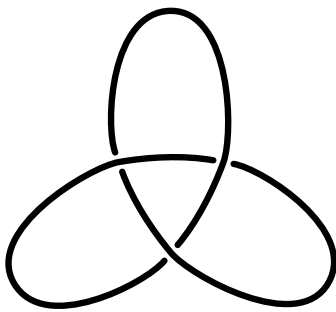
Let \mathcal{T} be a one-vertex ideal triangulation of the complement of K , so that each edge e in \mathcal{T} forms an arc α that meets K at its endpoints (and nowhere else). We call e a **tunnel edge** if the complement of $K \cup \alpha$ is a genus-2 handlebody; assuming that K is not the unknot, the existence of a tunnel edge implies that K has tunnel number equal to one.

Conjecture 2. *Let K be a knot with tunnel number equal to one. Then every one-vertex ideal triangulation of the complement of K has a tunnel edge.*

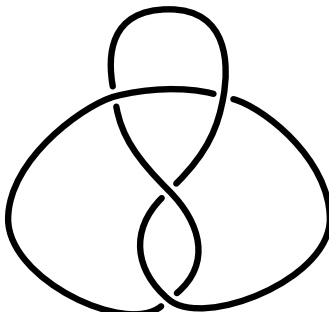
For the third conjecture, we consider **Seifert fibre spaces**. These are 3-manifolds that are fibred by circles in a particular way (see section 2.6 for a complete definition); we call each circle fibre a **Seifert fibre**. Seifert fibre spaces are important because they play a central role in canonical torus decompositions for closed orientable irreducible 3-manifolds:

- The JSJ decomposition (due to Jaco and Shalen [19], and Johannson [21]) cuts such 3-manifolds into pieces that are either atoroidal or Seifert fibred.

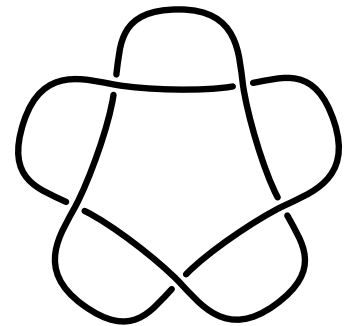
¹Lackenby and Schleimer use a slightly different definition of prism manifold than the one we give in section 2.6.



(a) The trefoil knot.



(b) The figure-eight knot.



(c) The $(5, 2)$ torus knot.

Figure 1: Three knots with tunnel number equal to one.

- The geometric decomposition from Thurston’s geometrisation conjecture (famously proved by Perelman [28, 30, 29]) cuts such 3-manifolds into pieces that are either hyperbolic or graph manifolds; the graph manifolds are precisely the 3-manifolds that can be further decomposed along tori into Seifert fibre spaces.

The **small** Seifert fibre spaces do not contain any embedded two-sided incompressible surfaces, which makes them relatively difficult to work with.

Conjecture 3. *Every one-vertex triangulation of a small Seifert fibre space has an edge isotopic to a Seifert fibre.*

1.2 Using a targeted search to find counterexamples

As mentioned earlier, we have found counterexamples to all three conjectures listed in section 1.1. Our focus for the rest of this paper will mainly be on the methods that we used to find these counterexamples. The key innovation is a heuristic for measuring how “far away” a triangulation is from having no core edges (or more generally, no edges satisfying any particular topological property that is computable).

To see why such a heuristic is necessary, consider the 3-sphere—the simplest possible lens space; for the 3-sphere, core edges are equivalent to edges that are **unknotted**. In the census of all triangulations with up to 10 tetrahedra, there are 422 533 279 one-vertex triangulations of the 3-sphere. We tested all of these and found that they all have at least one core edge. This required just over 22 hours of wall time running on 12 threads in parallel, but this does not include the time required to:

- (1) generate the census in the first place; and
- (2) identify all the 3-spheres in this census (which had been done previously [4, 5]).

(We also performed a more exhaustive test—requiring about 53 and a half hours of wall time on 12 parallel threads—which showed that all of the one-vertex 3-spheres with up to 10 tetrahedra actually have at least *two* core edges.)

The main takeaway is that this exhaustive search was both expensive and unsuccessful. In contrast, by using our heuristic to enumerate triangulations in a targeted fashion, we were able to find all of our counterexamples in just *minutes* of wall time, without ever needing to pre-process large quantities of data. It is also worth noting that all of our counterexamples have at least 11 tetrahedra, putting them beyond the limits of the census. See section 5 for detailed computational results; at the end of section 5, we also show how to turn each of our counterexamples into an infinite family.

We discuss the key tools and algorithms that allowed us to find these examples in sections 3 and 4. Specifically, section 4 introduces our heuristic and our targeted search algorithm. Section 3 discusses a number of auxiliary algorithms, all of which may be of independent interest; in particular, we present (and implement) an improved algorithm for handlebody recognition in section 3.1.

We finish with section 6, which raises some questions that remain unanswered. In particular, in section 6.2, we mention some other potential applications of the idea of using heuristics to selectively enumerate large triangulations.

2 Preliminaries

2.1 Triangulations

A (generalised) **triangulation** \mathcal{T} is a finite collection of tetrahedra whose triangular faces may be affinely identified in pairs; each equivalence class of such faces is a **face** of \mathcal{T} . The **size** of \mathcal{T} , denoted $|\mathcal{T}|$, is the number of tetrahedra that make up \mathcal{T} . The **boundary** of \mathcal{T} consists of all the faces that are not identified with any other faces. If the boundary is empty, we say that \mathcal{T} is **closed**; otherwise, we say that \mathcal{T} is **bounded**. We allow faces of the same tetrahedron to be identified, which means that our triangulations need not be simplicial complexes.

As a result of the face identifications, many edges and vertices of the tetrahedra may also become identified. The resulting equivalence classes of edges are called **edges** of the triangulation; similarly, the resulting equivalence classes of vertices are called **vertices** of the triangulation. The **degree** of an edge e of a triangulation is the number of tetrahedra that meet e , counted with multiplicity; this is equivalent to the number of tetrahedron edges that are identified to form e . The **1-skeleton** of a triangulation \mathcal{T} is the subcomplex consisting only of the vertices and edges of \mathcal{T} .

If a point lies on the boundary of a triangulation, then we say that it is **boundary**; otherwise, we say that it is **internal**. If a face, edge or vertex consists *entirely* of boundary points, then we say that it is **boundary**; otherwise, we say that it is **internal**.

A notable feature of generalised triangulations is that it is possible to get a **one-vertex triangulation**: a triangulation in which all of the tetrahedron vertices are identified to form a single vertex. In fact, *every* compact 3-manifold with at most one boundary component admits a one-vertex triangulation; one way to prove this is to use the two-tetrahedron “triangular-pillow-with-tunnel” that was first introduced by Weeks [13, 38].

As a small but informative example, we build a one-vertex triangulation \mathcal{T} of the solid torus using just a single tetrahedron Δ . Label the vertices of Δ by 0, 1, 2 and 3, as shown in Figure 2. Glue the front two faces so that vertices 0, 1 and 2 of the left face are respectively identified with vertices 1, 3 and 0 of the right face. Although \mathcal{T} is not a simplicial complex, it is a perfectly sensible triangulation in the sense we have just defined. Observe that all four vertices of Δ get identified to become a single boundary vertex in \mathcal{T} , and that \mathcal{T} has three edges (all of which are boundary) given by identifying the following edges of Δ :

- edges 20, 01 and 13 all form a single edge, as indicated by the black arrows in Figure 2;
- edges 12 and 30 together form a single edge, as indicated by the white arrows in Figure 2; and
- edge 23 forms the final edge.

One way to see that \mathcal{T} does indeed triangulate the solid torus is to observe that the internal face of \mathcal{T} forms a Möbius band; we can then think of the whole triangulation as a “thickening” of this Möbius band, which is a solid torus.

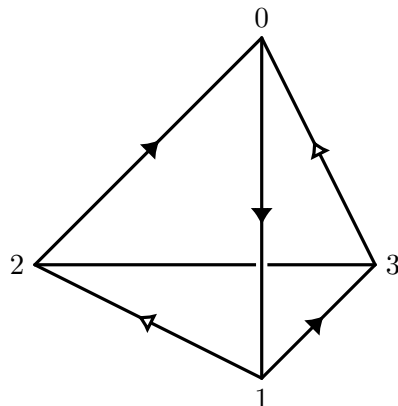


Figure 2: Gluing two faces of a single tetrahedron with a “twist” gives a one-vertex triangulation of the solid torus.

In general, for a triangulation \mathcal{T} to represent a 3-manifold, every point p in \mathcal{T} must be **non-singular** in the sense that it has a small neighbourhood bounded by either a disc (if p is boundary) or a 2-sphere (if p is internal). This condition may fail to hold for vertices and midpoints of edges. For this paper, we insist that no edge is ever identified with itself in reverse; this ensures that midpoints of edges are always non-singular.

We call \mathcal{T} a **3-manifold triangulation** if all its vertices are non-singular, because in this case \mathcal{T} will genuinely be a 3-manifold (possibly with boundary). However, we also allow vertices to be **ideal**, meaning that a small neighbourhood of the vertex is bounded by a closed surface other than the 2-sphere. **Ideal triangulations** (which contain one or more ideal vertices) often give an efficient way to represent the 3-manifold with boundary that is obtained by truncating the ideal vertices; this idea originated with Thurston's two-tetrahedron ideal triangulation of the figure-eight knot complement [37, Example 1.4.8].

To concretely encode a triangulation, we usually give each tetrahedron both a label and an ordering of its four vertices. Two triangulations are (**combinatorially**) **isomorphic** if they are identical up to relabelling tetrahedra and/or reordering tetrahedron vertices. We can uniquely identify any isomorphism class of triangulations using a short, efficiently-computable string called an **isomorphism signature**. There are many ways to formulate isomorphism signatures; we use the formulation described in [5], which is implemented in `Regina` [6, 9].

2.2 The 2-3 and 3-2 moves

Given any one-vertex triangulation \mathcal{T} with at least two tetrahedra, we can produce a new one-vertex triangulation of the same 3-manifold by performing a **2-3 move** about a (triangular) face that meets two distinct tetrahedra; this move replaces these two tetrahedra with three tetrahedra attached around a new edge e , as illustrated in Figure 3. We call the inverse move a **3-2 move** about the edge e . Observe that it is possible to perform a 3-2 move about an edge if and only if this edge is an internal degree-3 edge that actually meets three distinct tetrahedra.

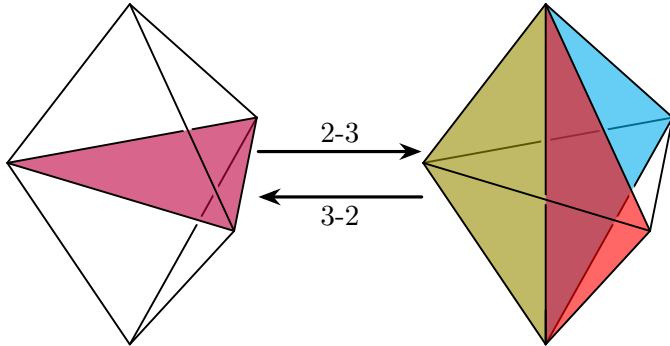


Figure 3: The 2-3 and 3-2 moves.

With this in mind, consider a closed 3-manifold \mathcal{M} . We can think of the one-vertex triangulations of \mathcal{M} with at least two tetrahedra as nodes of an infinite graph, with two nodes connected by an undirected arc if and only if the corresponding triangulations are related by a 2-3 move; this graph is called the **Pachner graph** of \mathcal{M} . Matveev [26] and Piergallini [31] independently proved the following result (though they did not state this result in terms of Pachner graphs):

Theorem 4. *For every closed 3-manifold \mathcal{M} , the Pachner graph of \mathcal{M} is connected.*

An analogous result holds for one-vertex ideal triangulations, as a special case of a theorem due to Amendola [1]. An alternative proof of Amendola's theorem can also be found in [33].

Since we are particularly interested in the *edges* of one-vertex triangulations, it is worth emphasising how the 2-3 and 3-2 moves affect the 1-skeleton of a triangulation. A 2-3 move creates a new edge, but otherwise leaves the 1-skeleton untouched. A 3-2 move about an edge e removes this edge, but otherwise leaves the 1-skeleton untouched.

2.3 Embedded surfaces

We can often learn a lot about a 3-manifold by looking at the embedded surfaces that it contains. Here, we review some standard terminology for such surfaces.

Throughout this section, let S denote a surface embedded in a compact 3-manifold \mathcal{M} (possibly with boundary). We say that S is **properly** embedded in \mathcal{M} if $S \cap \partial\mathcal{M} = \partial S$.

If S is a 2-sphere, then we say that S is **inessential** if it bounds a 3-ball in \mathcal{M} , and **essential** otherwise. The 3-manifold \mathcal{M} is **reducible** if it contains an essential 2-sphere, and **irreducible** otherwise.

A disc D embedded in \mathcal{M} is a **compressing disc** for S if $D \cap S = \partial D$. Such a compressing disc D is **inessential** if the curve ∂D bounds another disc that lies entirely inside S ; otherwise, D is **essential**. Figure 4 illustrates an inessential compressing disc. The surface S is **compressible** if it admits an essential compressing disc, and **incompressible** otherwise. In the special case where the surface S is just $\partial\mathcal{M}$, notice that a compressing disc for S is the same thing as a properly embedded disc in \mathcal{M} ; thus, whenever we are working with a *properly* embedded disc D , we will also often refer to D as a compressing disc (without needing to specify the surface $\partial\mathcal{M}$). If $\partial\mathcal{M}$ is compressible, then we say that \mathcal{M} is **∂ -reducible**; otherwise, \mathcal{M} is **∂ -irreducible**.

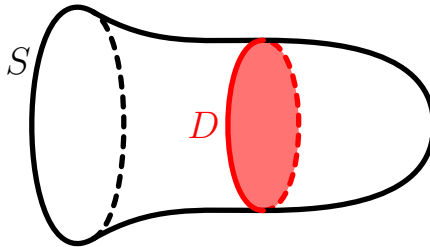


Figure 4: An inessential compressing disc D for a surface S .

We say that \mathcal{M} is **sufficiently large** if it contains a two-sided incompressible surface other than S^2 (the 2-sphere) or \mathbb{RP}^2 (the real projective plane); otherwise, \mathcal{M} is **small**. We say that \mathcal{M} is **Haken** if it is irreducible, ∂ -irreducible and sufficiently large; otherwise, \mathcal{M} is **non-Haken**. The terms “small” and “non-Haken” are sometimes used interchangeably because it is very common to work exclusively with 3-manifolds that are irreducible and ∂ -irreducible.

Suppose, for this paragraph, that S has non-empty boundary and is properly embedded. A disc D embedded in \mathcal{M} is a **∂ -compressing disc** for S if there are two arcs α and β such that $\alpha = D \cap S$, $\beta = D \cap \partial\mathcal{M}$, $\alpha \cup \beta = \partial D$, and $\alpha \cap \beta = \partial\alpha = \partial\beta$. Such a ∂ -compressing disc D is **inessential** if there is another arc γ in ∂S such that $\alpha \cap \gamma = \partial\alpha = \partial\gamma$ and the curve $\alpha \cup \gamma$ bounds another disc that lies entirely inside S ; otherwise, D is **essential**. Figure 5 illustrates an inessential ∂ -compressing disc. The surface S is **∂ -compressible** if it admits an essential ∂ -compressing disc, and **∂ -incompressible** otherwise.

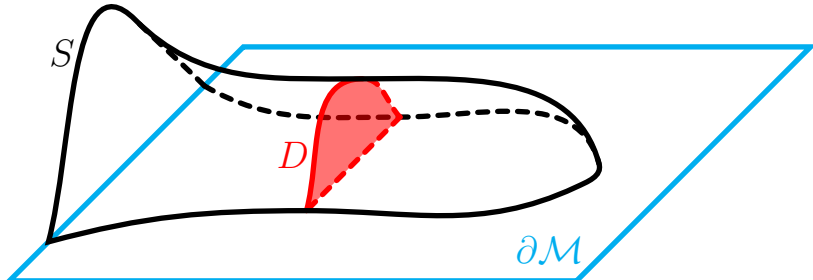


Figure 5: An inessential ∂ -compressing disc D for a surface S .

Finally, suppose S is properly embedded. We say that S is **boundary parallel** if there is an isotopy fixing ∂S that sends S to a subsurface of $\partial\mathcal{M}$. In the case where S is neither a 2-sphere nor a disc, we say that S is **essential** if it is incompressible, ∂ -incompressible, and not boundary parallel.

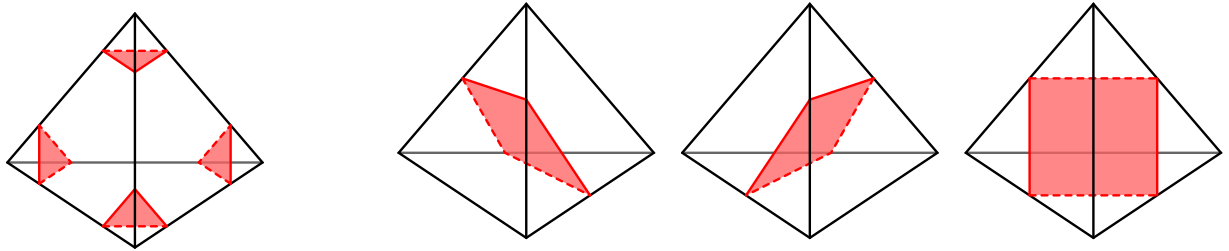
2.4 Normal surfaces

As we discuss in sections 3.1 and 3.2, our work relies on a number of results from normal surface theory. Here, we only outline the ideas that are required for our purposes; see [15] and [18] for more comprehensive overviews.

A (possibly disconnected) properly embedded surface S in a 3-manifold triangulation \mathcal{T} is a **normal surface** if:

- S meets each simplex (i.e., vertex, edge, triangle, or tetrahedron) of \mathcal{T} transversely; and
- S meets each tetrahedron Δ of \mathcal{T} in a finite (and possibly empty) collection of discs—known as **elementary discs**²—where each such disc is a curvilinear triangle or quadrilateral whose vertices lie on different edges of Δ .

Up to **normal isotopy** (i.e., an ambient isotopy that preserves every simplex of \mathcal{T}), every elementary disc has one of the seven types shown in Figure 6.



(a) The four triangle types. (b) The three quadrilateral types.

Figure 6: The seven elementary disc types in a tetrahedron.

The simplest example of a normal surface is a **vertex-linking surface**, which consists entirely of triangles. Such surfaces always exist, so finding these surfaces never gives us any new information about the underlying 3-manifold. For this reason, we consider a normal surface to be **non-trivial** when it includes at least one quadrilateral piece.

If \mathcal{T} is an n -tetrahedron triangulation, then we can represent any normal surface in \mathcal{T} as a **normal coordinate** vector in \mathbb{R}^{7n} that counts the number of elementary discs of each type in each tetrahedron. Conversely, it turns out that the space of vectors in \mathbb{R}^{7n} that correspond to normal surfaces in \mathcal{T} can be described by a collection of combinatorial constraints (namely, the **quadrilateral constraints**) together with a collection of homogeneous linear inequalities. By homogeneity, every solution to these linear inequalities is a scalar multiple of a vector in a convex polytope $\mathcal{P}(\mathcal{T}) \subset \mathbb{R}^{7n}$.

Given two normal surfaces S and S' , we can consider the sum of the two corresponding normal coordinate vectors. Provided the quadrilateral constraints are still satisfied, this gives a new normal surface called the **(Haken) sum** of S and S' , denoted $S + S'$. In particular, we can always take the sum of a normal surface S with itself k times, for some positive integer k ; we denote this surface by kS . An important special case is the surface $2S$, which we call the **double** of S .

As we will see in sections 3.1 and 3.2, it is often sufficient to focus our attention on the normal surfaces that arise as minimal scalar multiples of vertices of the polytope $\mathcal{P}(\mathcal{T})$ (by “minimal”, we mean the smallest scalar multiple such that the coordinates are all integers); such surfaces are called **vertex normal surfaces**³. Roughly, the significance of vertex normal surfaces is that they form a finite and algorithmically enumerable “basis” for the set of all normal surfaces.

²Some authors use the term “normal disc” (for instance, see [18]). We reserve the term “normal disc” to refer to a normal surface that forms a properly embedded disc.

³Some authors use different terminology. For instance, in [20], vertex normal surfaces are called “vertex solutions”, and the term “vertex surface” refers to a connected *two-sided* normal surface that is either a vertex solution or the double of a vertex solution.

2.5 Lens spaces

We now give a brief review of lens spaces, which will also allow us to specify the conventions that we use. There are several equivalent ways to define lens spaces. The most convenient way for our purposes is to construct them by gluing together two solid tori.

We can perform any such gluing by first attaching a thickened disc along a non-trivial circle γ in the boundary of one of the solid tori. To complete the gluing, we just need to fill the resulting 2-sphere boundary with a 3-ball. Since there is only one way to fill with a 3-ball, the gluing is completely determined by the choice of the circle γ .

Thus, we can parametrise all possible lens spaces by parametrising all possible choices for γ . To this end, view each solid torus as a product $D^2 \times S^1$. Up to isotopy, every non-trivial circle in the boundary torus $\partial D^2 \times S^1$ lifts to a straight line of either rational or infinite slope in the universal cover \mathbb{R}^2 , and we can parametrise such circles by this slope; our convention here will be that a circle of the form $\{x\} \times S^1$ has slope ∞ , while a circle of the form $\partial D^2 \times \{y\}$ has slope 0.

With all this in mind, define the **lens space** $L_{p,q}$ to be the 3-manifold given by taking the slope of γ to be $\frac{p}{q}$ in the above construction.⁴ This parametrisation is not unique: it turns out that $L_{p,q}$ and $L_{p',q'}$ are homeomorphic if and only if $|p'| = |p|$ and $q' \equiv \pm q^{\pm 1} \pmod{p}$ [3]. Some authors exclude degenerate cases—most commonly, the 3-sphere ($L_{1,0}$) and/or $S^2 \times S^1$ ($L_{0,1}$)—from their definition of lens spaces; we make no such restrictions here.

2.6 Seifert fibre spaces

We now give a quick review of Seifert fibre spaces, which will also allow us to establish some notation. There are many sources for more comprehensive discussion of Seifert fibre spaces; much of the material here is based on the discussion in Hatcher's 3-manifold notes [16], but with simplifications in places where it is not necessary to discuss the theory in full generality.

We begin by constructing fibred solid tori. Take the cylinder $D^2 \times [0, 1]$, and form a solid torus by gluing the discs $D^2 \times \{0\}$ and $D^2 \times \{1\}$ together with a $\frac{2\pi p}{q}$ rotation, where q is a positive integer, and p is any integer coprime with q . This solid torus is fibred by circles in the following way:

- There is a fibre $\{0\} \times S^1$ given by closing up the segment $\{0\} \times [0, 1]$.
- The remaining fibres are given by joining together q segments of the form $\{x\} \times [0, 1]$.

We call this solid torus (with this fibration) a **fibred solid torus with multiplicity q** .

A **Seifert fibre space** is a 3-manifold that is fibred by circles in such a way that each circle fibre—called a **Seifert fibre**—has a small solid torus neighbourhood that forms a fibred solid torus⁵. If the multiplicity of the fibred solid torus neighbourhood is one, then we call the Seifert fibre a **regular fibre**; otherwise, we call the Seifert fibre an **exceptional fibre**⁶. The exceptional fibres are isolated, and they are disjoint from the boundary of the manifold.

Consider a compact Seifert fibre space \mathcal{M} , and let k be the (necessarily finite) number of exceptional fibres in \mathcal{M} . By removing a small solid torus neighbourhood of each exceptional fibre, we obtain a circle bundle \mathcal{M}' over a surface B' ; the surface B' has k boundary components corresponding to the exceptional fibres that we removed (and possibly some additional boundary components corresponding to boundary components of \mathcal{M}). Let B be the surface obtained by filling these k boundary components of B' with discs; we say that \mathcal{M} is **(Seifert) fibred over B** , and we call B the **base surface**.

From this point onwards, we restrict our attention to Seifert fibre spaces that are compact, connected, orientable and irreducible. The irreducibility restriction only rules out three examples:

- $S^2 \times S^1$ (product of the 2-sphere S^2 and the circle S^1),
- $S^2 \times S^1$ (twisted product of S^2 and S^1), and
- $\mathbb{R}P^3 \# \mathbb{R}P^3$ (connected sum of two copies of real projective space $\mathbb{R}P^3$).

⁴With the conventions we have chosen here, this is equivalent to saying that $L_{p,q}$ is obtained by $\frac{p}{q}$ Dehn surgery on the unknot.

⁵Some authors also allow fibred solid Klein bottle neighbourhoods (for instance, see [35]).

⁶Other authors use various other names for exceptional fibres, such as *multiple fibres* [16] or *critical fibres* [35].

We now say some words about the incompressible, ∂ -incompressible surfaces⁷ in a Seifert fibre space \mathcal{M} (with the restrictions just mentioned). We call an embedded surface in \mathcal{M} **vertical** if it consists of a union of regular fibres, and **horizontal** if it meets all fibres transversely. Up to isotopy, every incompressible, ∂ -incompressible surface in \mathcal{M} is either vertical or horizontal. In the other direction, every connected two-sided horizontal surface is incompressible and ∂ -incompressible. However, this is not quite true for vertical surfaces:

- if a vertical torus bounds a fibred solid torus, then it is compressible; and
- if a vertical annulus cuts off from \mathcal{M} a solid torus with the product fibration, then it is ∂ -compressible.

It turns out that these are the only exceptions; every other connected two-sided vertical surface is incompressible and ∂ -incompressible.

Suppose, in addition to the restrictions mentioned earlier, that the Seifert fibre space \mathcal{M} is closed. As mentioned in section 1.1, we are particularly interested in the case where \mathcal{M} is *small* (recall from section 2.3 that this means that \mathcal{M} contains no two-sided incompressible surfaces other than S^2 or \mathbb{RP}^2).⁸ It turns out that we can always find an incompressible vertical torus in \mathcal{M} unless either:

- \mathcal{M} is fibred over S^2 with at most three exceptional fibres; or
- \mathcal{M} is fibred over \mathbb{RP}^2 with at most one exceptional fibre.

In other words, if \mathcal{M} is small, then it must be fibred in one of these two ways (but the converse is not true, because a 3-manifold that is fibred in this way can still contain two-sided incompressible *horizontal* surfaces).

Consider the case where \mathcal{M} is fibred over \mathbb{RP}^2 with at most one exceptional fibre. If there are no exceptional fibres, then \mathcal{M} must actually be homeomorphic to $\mathbb{RP}^3 \# \mathbb{RP}^3$; this is one of the reducible cases that we chose to ignore earlier. If there is one exceptional fibre (still with base surface \mathbb{RP}^2), then \mathcal{M} is a **prism manifold**⁹. For various reasons, prism manifolds are often treated as a special case in the literature. One of the reasons is that prism manifolds also admit a fibration over S^2 with three exceptional fibres (we will say more about this shortly). Since we are looking for triangulations with no edges isotopic to Seifert fibres, the existence of multiple Seifert fibrations is a little inconvenient for our purposes, so we will usually exclude prism manifolds from our discussions.

We now consider the case where \mathcal{M} is fibred over S^2 with at most *two* exceptional fibres. In this case, \mathcal{M} is a lens space, and it has *infinitely* many Seifert fibrations. For this reason, we will also usually exclude lens spaces when we are working with small Seifert fibre spaces.

This leaves the case where \mathcal{M} is fibred over S^2 with exactly three exceptional fibres. Apart from the prism manifolds mentioned earlier, these all have a unique Seifert fibration. The following construction gives a natural way to parametrise these Seifert fibre spaces:

Construction 5 (Seifert fibre spaces with base surface S^2 and three exceptional fibres). *Take the circle bundle $P \times S^1$, where P is a **pair of pants** (i.e., a 2-sphere with three small discs removed), and glue a solid torus to each of the three torus boundary components of our circle bundle.*

We specify the three gluings by their slopes (similar to how we constructed lens spaces in section 2.5). To ensure that the slopes are well-defined, fix an orientation of $P \times S^1$. Letting b_0, b_1 and b_2 denote the circles that form the boundary components of P , fix any particular $i \in \{0, 1, 2\}$ and consider the torus boundary component $b_i \times S^1$. Here, we use the convention that a circle of the form $b_i \times \{y\}$ has slope 0, and any fibre in $b_i \times S^1$ (which is of the form $\{x\} \times S^1$) has slope ∞ . Any gluing of a solid torus \mathcal{T} to $b_i \times S^1$ is completely determined by the slope of a non-trivial circle along which we attach a meridian disc of \mathcal{T} , so we can parametrise the gluing by this slope.

Letting $\frac{\alpha_i}{\beta_i} \in \mathbb{Q}$ (with $\beta_i > 0$ and $\gcd(\alpha_i, \beta_i) = 1$) denote the slope by which we glue a solid torus \mathcal{T} to $b_i \times S^1$, we can extend the fibration on the circle bundle $P \times S^1$ so that \mathcal{T} becomes a fibred solid torus

⁷In his 3-manifold notes, Hatcher calls these surfaces “essential” [16, p. 18]. We do not use this terminology because, as defined in section 2.3, we require that essential surfaces are not boundary parallel.

⁸In the specific context of Seifert fibre spaces, some authors take “small” to mean that we have base surface S^2 and at most three exceptional fibres (for instance, see [24]).

⁹This terminology is consistent with [35]. Other authors define prism manifolds differently (for instance, see [23]).

of multiplicity β_i . Thus, provided we glue all three solid tori via non-integer slopes, the 3-manifold that results from this construction will be fibred over S^2 with exactly three exceptional fibres; throughout this paper, we will denote this Seifert fibre space by $\mathcal{S}\left(\frac{\alpha_0}{\beta_0}, \frac{\alpha_1}{\beta_1}, \frac{\alpha_2}{\beta_2}\right)$.

The parametrisation given at the end of Construction 5 is not unique; see Proposition 2.1 of [16] for a precise description of when two such parametrisations describe the same Seifert fibration.

We also mentioned earlier that it is possible for a 3-manifold to be Seifert fibred in more than one way. In particular, we noted that for base surface S^2 and three exceptional fibres, such non-uniqueness only occurs for the prism manifolds. We can now describe this non-uniqueness more precisely: in addition to being fibred over \mathbb{RP}^2 with one exceptional fibre, each prism manifold also admits a Seifert fibration of the form $\mathcal{S}\left(\frac{1}{2}, -\frac{1}{2}, \frac{\alpha}{\beta}\right)$.

3 Key tools

This section discusses some new algorithms and implementations that were crucial for our work. We anticipate that these algorithms may be useful for other purposes.

3.1 Handlebody recognition

To find counterexamples to Conjectures 1 and 2, we need to have algorithms to recognise solid tori and genus-2 handlebodies. **Regina** includes an implementation of solid torus recognition [14, 20] that is remarkably efficient in practice [9, 6, 11]. We generalise this to recognise handlebodies of arbitrary genus, improving the earlier algorithm of Jaco and Tollefson [20, Algorithm 9.3].

The following theorem—which is an immediate consequence of Corollary 6.4 of [20], due to Jaco and Tollefson—lies at the heart of our handlebody recognition algorithm:

Theorem 6. *Let \mathcal{T} be a triangulation of a compact irreducible 3-manifold with compressible boundary. Then \mathcal{T} contains a vertex normal surface that realises an essential compressing disc.*

Note that handlebodies satisfy the conditions for this theorem. With this in mind, the basic strategy of our algorithm is to repeatedly cut along vertex normal compressing discs; a triangulation \mathcal{T} is a handlebody if and only if doing this eventually decomposes \mathcal{T} into a collection of 3-balls. For computational reasons, we modify this approach in two ways.

First, we expand our focus beyond discs, to include any vertex normal surface S whose Euler characteristic $\chi(S)$ is positive. The rationale is that $\chi(S)$ can be expressed as a linear function in normal coordinates, which allows us to exploit linear programming techniques. This leads to an algorithm for detecting non-trivial normal spheres and discs that is fast in practice (even though, in theory, this is actually the exponential-time bottleneck for both solid torus recognition and handlebody recognition); see [11] for details.

Second, because cutting along a normal surface can increase the number of tetrahedra exponentially, we instead use a technique called **crushing**. Crushing was first developed by Jaco and Rubinstein [18], following earlier unpublished work of Casson, and was later refined by the first author [7]. Crushing a non-trivial normal surface has the following crucial benefit: it is guaranteed to produce a new triangulation with strictly fewer tetrahedra than before. The trade-off is that crushing a normal sphere or disc could have topological side-effects, as detailed in the following theorem (this is a restatement of Theorem 2 of [7], which is itself a summary of a series of results from [18]):

Theorem 7. *Let \mathcal{T} be a triangulation of a compact orientable 3-manifold \mathcal{M} , and let S be a normal sphere or disc in \mathcal{T} . Crushing S yields a triangulation \mathcal{T}' whose underlying 3-manifold \mathcal{M}' is obtained from \mathcal{M} by a finite (and possibly empty) sequence of the following operations:*

- *undoing connected sums;*
- *cutting along properly embedded discs;*
- *filling boundary 2-spheres with 3-balls; and*
- *deleting 3-ball, 3-sphere, \mathbb{RP}^3 , $L_{3,1}$ or $S^2 \times S^1$ components.*

For the rest of this section, call a connected orientable 3-manifold **interesting** if:

- it has exactly one boundary component; and
- its first homology is \mathbb{Z}^g , where g is the genus of the boundary surface.

In other words, we consider a 3-manifold \mathcal{M} to be interesting if it has the same basic properties as a handlebody, which means that we need more sophisticated techniques to decide whether \mathcal{M} is a handlebody. In analogy with homology spheres, one could also say that an interesting 3-manifold is a “homology handlebody”. Our handlebody recognition algorithm relies on the following consequence of Theorem 7:

Proposition 8. *Let \mathcal{T} be a triangulation of an interesting 3-manifold, and suppose that \mathcal{T} contains a non-trivial normal sphere or disc S . Let \mathcal{T}' denote the triangulation obtained by crushing S . Then each component of \mathcal{T}' is either closed or interesting. Moreover, \mathcal{T} is a handlebody if and only if every component of \mathcal{T}' is either a 3-sphere or a handlebody.*

Proof. The underlying 3-manifold of \mathcal{T}' is obtained from the underlying 3-manifold of \mathcal{T} by performing some sequence of the operations listed in Theorem 7. Thus, to prove the proposition, it suffices to consider each of these operations one at a time.

In more detail, let \mathcal{M} be an orientable 3-manifold that is either closed or interesting, and let \mathcal{M}' be the 3-manifold obtained from \mathcal{M} by performing any one of the operations listed in Theorem 7. We will prove the following two claims:

- The components of \mathcal{M}' are all either closed or interesting.
- The 3-manifold \mathcal{M} is either a 3-sphere or a handlebody if and only if every component of \mathcal{M}' is either a 3-sphere or a handlebody.

Our proposition follows from these claims by induction on the number of operations from Theorem 7 that we perform.

We begin with the case where \mathcal{M} is closed, since in this case there are only two possibilities, both of which are straightforward:

- If \mathcal{M} is a copy of S^3 , $L_{3,1}$ or $S^2 \times S^1$, then we might delete \mathcal{M} entirely, in which case \mathcal{M}' is empty.¹⁰
- We might undo a connected sum, in which case \mathcal{M}' consists of two closed components. In this case, \mathcal{M} is a 3-sphere if and only if both components of \mathcal{M}' are 3-spheres.

With that out of the way, we devote the rest of this proof to the case where \mathcal{M} is interesting. We start with the two easy cases:

- If \mathcal{M} is a 3-ball, then we might delete \mathcal{M} entirely, in which case \mathcal{M}' is empty.
- If \mathcal{M} has sphere boundary, then we might fill this sphere with a 3-ball, in which case \mathcal{M}' is closed. Moreover, \mathcal{M} is a 3-ball if and only if \mathcal{M}' is a 3-sphere.

It remains to consider what happens if we either undo a connected sum, or cut along a properly embedded disc. For these remaining cases, let g denote the genus of the boundary surface $\partial\mathcal{M}$.

Suppose we undo a connected sum. In this case, since \mathcal{M} has exactly one boundary component, \mathcal{M}' has two components: a closed component \mathcal{C} , and a component \mathcal{B} with the same boundary as \mathcal{M} . Since $H_1(\partial\mathcal{B})$ has rank $2g$, we know that $H_1(\mathcal{B})$ has rank at least g (see Lemma 3.5 of [16]). Since

$$H_1(\mathcal{B}) \oplus H_1(\mathcal{C}) \simeq H_1(\mathcal{B} \# \mathcal{C}) \simeq H_1(\mathcal{M}) \simeq \mathbb{Z}^g,$$

we conclude that $H_1(\mathcal{B}) \simeq \mathbb{Z}^g$, and hence that \mathcal{B} is interesting. Moreover, \mathcal{M} is a handlebody if and only if \mathcal{C} is a 3-sphere and \mathcal{B} is a handlebody.¹¹

¹⁰Actually, because we have assumed that the initial triangulation \mathcal{T} is interesting, it is possible to prove that the only closed components we will ever encounter are 3-manifolds with trivial first homology; thus, the $L_{3,1}$ and $S^2 \times S^1$ cases are actually impossible. However, this detail is not important for our proof.

¹¹Here, it is crucial that \mathcal{M} has exactly one boundary component, as this rules out the case where \mathcal{M} is a connected sum of two handlebodies (otherwise, it would be possible for \mathcal{M}' to be the disjoint union of these two handlebodies, even though \mathcal{M} is not itself a handlebody). Later in the proof, we will see why it is necessary to make the stronger assumption that \mathcal{M} is actually interesting.

On the other hand, suppose we cut along a properly embedded disc D . We first consider the case where D is a separating disc. In this case, \mathcal{M}' has two components \mathcal{B}_1 and \mathcal{B}_2 , each with a single boundary component. For each $i \in \{1, 2\}$, let g_i denote the genus of the boundary surface $\partial\mathcal{B}_i$; note that $H_1(\mathcal{B}_i)$ has rank at least g_i . By retracting D to a point, we see that \mathcal{M} is homotopy-equivalent to the wedge sum $\mathcal{B}_1 \vee \mathcal{B}_2$, and hence that

$$H_1(\mathcal{B}_1) \oplus H_1(\mathcal{B}_2) \simeq H_1(\mathcal{B}_1 \vee \mathcal{B}_2) \simeq H_1(\mathcal{M}) \simeq \mathbb{Z}^g.$$

From this, together with the fact that $g = g_1 + g_2$, we conclude that \mathcal{B}_1 and \mathcal{B}_2 are both interesting. Moreover, \mathcal{M} is a handlebody if and only if \mathcal{B}_1 and \mathcal{B}_2 are both handlebodies.

All that remains is to consider the case where D is non-separating, in which case \mathcal{M}' consists of a single component with boundary. This case requires much more work than the others. We begin by noting that \mathcal{M} is a handlebody if and only if \mathcal{M}' is a handlebody. Thus, the rest of this proof is entirely devoted to showing that \mathcal{M}' is interesting. The first step is to show that ∂D is a non-separating curve on the boundary surface $\partial\mathcal{M}$, as this will imply that \mathcal{M}' has a single boundary component.¹²

Suppose instead that ∂D separates $\partial\mathcal{M}$ into two pieces P and Q . Let h denote the genus of P . Since D is a non-separating disc, there is a closed loop γ in the interior of \mathcal{M} that meets D exactly once. Push $P \cup D$ slightly off the boundary to obtain a closed genus- h surface S that meets γ exactly once. Let X' be a small neighbourhood of $S \cup \gamma$, and let $Y' = \mathcal{M} \setminus X'$. The boundary of X' is a surface of genus $2h$; let N be a small neighbourhood of this surface. Taking $X = X' \cup N$ and $Y = Y' \cup N$ gives a pair of subspaces whose interiors together cover \mathcal{M} . Noting that $X \cap Y = N$, the Mayer-Vietoris sequence for X and Y gives us the following exact sequence:

$$\cdots \longrightarrow H_1(N) \xrightarrow{\varphi} H_1(X) \oplus H_1(Y) \xrightarrow{\psi} H_1(\mathcal{M}) \longrightarrow \cdots$$

$$\begin{array}{ccc} \downarrow & \downarrow & \downarrow \\ \mathbb{Z}^{4h} & \mathbb{Z}^{2h+1} \oplus H_1(Y) & \mathbb{Z}^g \end{array}$$

Moreover, since Y has two boundary components, one of genus g and the other of genus $2h$, we know that $H_1(Y)$ has rank at least $g + 2h$. Thus, in total, $H_1(X) \oplus H_1(Y)$ has rank at least $g + 4h + 1$. But we also know that $\text{im}(\psi)$ is free abelian with rank at most g , so exactness tells us that $\text{im}(\varphi)$ must have rank at least $4h + 1$. This is impossible, since $H_1(N)$ only has rank $4h$.

Thus, we see that ∂D must be a non-separating curve on $\partial\mathcal{M}$. This implies that \mathcal{M}' has exactly one boundary component, and that this boundary component has genus $g - 1$. To complete the proof, we just need to show that \mathcal{M}' is interesting by verifying that $H_1(\mathcal{M}') \simeq \mathbb{Z}^{g-1}$.

One way to do this is to examine the Mayer-Vietoris sequence for subspaces X and Y constructed as follows:

- Let X be a subspace of \mathcal{M} homeomorphic to \mathcal{M}' .
- Let Y be a 3-ball neighbourhood of the disc D .

We can choose X and Y so that their interiors together cover \mathcal{M} , and the intersection $N := X \cap Y$ is a disjoint pair of 3-balls. This gives the following exact sequence:

$$\cdots \longrightarrow H_1(N) \xrightarrow{\varphi_1} H_1(X) \oplus H_1(Y) \xrightarrow{\psi_1} H_1(\mathcal{M}) \xrightarrow{\partial} H_0(N) \xrightarrow{\varphi_0} H_0(X) \oplus H_0(Y) \xrightarrow{\psi_0} H_0(\mathcal{M}) \longrightarrow 0$$

$$\begin{array}{ccccccc} \downarrow & \downarrow & \downarrow & \downarrow & \downarrow & \downarrow & \downarrow \\ 0 & H_1(\mathcal{M}') & \mathbb{Z}^g & \mathbb{Z}^2 & \mathbb{Z}^2 & \mathbb{Z} & \mathbb{Z} \end{array}$$

By exactness, we know that:

- $H_1(\mathcal{M}') \simeq \ker(\partial)$; and
- $\text{im}(\psi_0)$, $\text{im}(\varphi_0)$ and $\text{im}(\partial)$ all have rank 1.

Thus, we see that $H_1(\mathcal{M}') \simeq \mathbb{Z}^{g-1}$, as required. \square

¹²Earlier, we pointed out that it is crucial that we never create a component with more than one boundary component. As we will see shortly, proving this in the present case requires the assumption that $H_1(\mathcal{M}) \simeq \mathbb{Z}^g$, which is why we need to assume that \mathcal{M} is interesting.

The last thing we rely on is an algorithm to recognise the 3-ball; this is a well-known variant of 3-sphere recognition [18, 32, 36], and an implementation is available in **Regina** [6, 9].

The following handlebody recognition algorithm is now also available in **Regina** [9]:

Algorithm 9 (Handlebody recognition). *To test whether a triangulation \mathcal{T} is a handlebody:*

- (1) *Check that \mathcal{T} is connected, orientable, and has exactly one boundary component. If \mathcal{T} fails to satisfy any of these conditions, then terminate and return `false`.*
- (2) *Compute the genus g of the boundary of \mathcal{T} .*
 - *In the case that $g = 0$, check whether \mathcal{T} is a 3-ball. If it is, terminate and return `true`; otherwise, terminate and return `false`.*
 - *In the case that $g > 0$, check whether the first homology of \mathcal{T} is \mathbb{Z}^g . If it is not, terminate and return `false`.*
- (3) *Create a list \mathcal{L} of triangulations to process, which initially contains \mathcal{T} (and nothing else). While \mathcal{L} is non-empty:*
 - (i) *Let \mathcal{F} be the first triangulation that appears in \mathcal{L} . Remove \mathcal{F} from \mathcal{L} .*
 - (ii) *Find a non-trivial normal sphere or disc S in \mathcal{F} . If no such surface exists, then terminate and return `false`.*
 - (iii) *Crush S . For each component \mathcal{C} of the triangulation \mathcal{R} that results from crushing:*
 - *If \mathcal{C} is closed, check whether \mathcal{C} is a 3-sphere. If it is, discard \mathcal{C} and move on to the next component of \mathcal{R} ; otherwise, terminate and return `false`.*
 - *If \mathcal{C} has sphere boundary, check whether \mathcal{C} is a 3-ball. If it is, discard \mathcal{C} and move on to the next component of \mathcal{R} ; otherwise, terminate and return `false`.*
 - *In any other case, add \mathcal{C} to the list \mathcal{L} , and move on to the next component of \mathcal{R} .*
- (4) *Once there are no more triangulations in \mathcal{L} , terminate and return `true`.*

Theorem 10 (Correctness). *Algorithm 9 correctly determines whether a given triangulation is a handlebody.*

Proof. Step (2) eliminates 3-manifolds with sphere boundary, and 3-manifolds that are not interesting. Thus, throughout this proof, we can safely assume that the initial triangulation \mathcal{T} represents an interesting 3-manifold whose boundary surface has positive genus.

We begin by proving that the algorithm terminates. It suffices to show that the loop in step (3) does not continue indefinitely. Indeed, each time we remove a triangulation \mathcal{F} from \mathcal{L} , we either crush a non-trivial normal surface S , or we terminate because there is no suitable surface S . Crushing S is guaranteed to reduce the number of tetrahedra, so even if we add some triangulations back into \mathcal{L} , the total number of tetrahedra in this list must decrease. This number cannot decrease indefinitely, so the algorithm must terminate.

We now prove that the algorithm correctly determines whether the input triangulation \mathcal{T} is a handlebody. The key is the following invariant, which is preserved every time we make a full pass through the loop in step (3): every triangulation in \mathcal{L} is interesting, and \mathcal{T} is a handlebody with positive genus if and only if every triangulation in \mathcal{L} is actually a handlebody with positive genus.

To prove that this invariant is indeed preserved, we first consider the case where the triangulation \mathcal{F} that we remove from \mathcal{L} is a handlebody with positive genus. In this case, Theorem 6 guarantees that we will find a non-trivial normal sphere or disc S in \mathcal{F} . Then, by Proposition 8, crushing S yields a new triangulation whose components are all either 3-spheres or handlebodies. We discard all the 3-spheres and 3-balls, leaving only handlebodies with positive genus. This suffices to show that the invariant is always preserved when the initial triangulation \mathcal{T} is a handlebody.

Suppose now that we remove a triangulation \mathcal{F} from \mathcal{L} that is not a handlebody. We need to check that the invariant is preserved if we pass through the loop without terminating and returning `false`. So, we can assume that we crush a non-trivial normal sphere or disc in \mathcal{F} , yielding a new triangulation \mathcal{F}' . We can also assume that all the closed components of \mathcal{F}' are 3-spheres, and that all the components of \mathcal{F}' with sphere boundary are 3-balls; we discard all such components. Proposition 8 tells us that the remaining components are all interesting, and that at least one of these remaining components is not a handlebody; we add all of these interesting components back into \mathcal{L} , thus ensuring

that \mathcal{L} still contains at least one triangulation that is not a handlebody. This shows that the invariant is always preserved when the initial triangulation \mathcal{T} is not a handlebody.

Altogether, we see that if \mathcal{T} is a handlebody, then the list \mathcal{L} must eventually become empty, in which case we terminate and correctly return `true`. On the other hand, if \mathcal{T} is not a handlebody, then \mathcal{L} can never become empty, so at some point we must terminate and correctly return `false`. \square

3.2 Detecting edges isotopic to Seifert fibres

To find counterexamples to Conjecture 3, we need to be able to take an edge e in a one-vertex triangulation of a small Seifert fibre space, and determine whether e is isotopic to a Seifert fibre. Since this is not easy to test conclusively, and since our main goal is to find a triangulation that definitely has no edges isotopic to Seifert fibres, we use an algorithm that only gives conclusive answers in one direction: certifying that an edge is *not* isotopic to a Seifert fibre.

Throughout this section, let \mathcal{T} be a one-vertex triangulation of an irreducible small Seifert fibre space that is neither a lens space nor a prism manifold, and fix an edge e of \mathcal{T} . (Recall from our discussion in section 2.6 that \mathcal{T} must be fibred over S^2 with three exceptional fibres, and that this is the unique Seifert fibration on \mathcal{T} .) The first step of our algorithm is to build a triangulation \mathcal{D} of the 3-manifold obtained by deleting a small solid torus neighbourhood of e . From here, our strategy is to take a list of normal surfaces that are guaranteed to occur in \mathcal{D} if e is isotopic to a Seifert fibre, and check whether all such surfaces occur in \mathcal{D} . This strategy appears to be effective as long as we use a sufficiently exhaustive list of surfaces.

The key theoretical result that we use is the following, which is a consequence of Corollary 6.8 of [20], due to Jaco and Tollefson:

Proposition 11. *Let \mathcal{F} be a triangulation of an orientable, compact, irreducible and ∂ -irreducible Seifert fibre space. Call a surface in \mathcal{F} **good** if it is essential, and is either a vertex normal surface or the double of a vertex normal surface.*

- *If \mathcal{F} has a vertical essential annulus, then it has a good vertical annulus.*
- *If \mathcal{F} has a vertical essential torus, then it has a good vertical torus. Moreover, if \mathcal{F} has more than one vertical essential torus (up to isotopy), then it has at least two good vertical tori.*

Proof. Suppose \mathcal{F} has a vertical essential annulus A . Corollary 6.8 of [20] tells us that A is isotopic to a normal annulus S such that for some $k \geq 1$, the surface kS is a sum of good annuli and good tori. Observe that at least one of the summands must be a good vertical annulus.

Suppose now that \mathcal{F} has a vertical essential torus A . This time, Corollary 6.8 of [20] tells us that A is isotopic to a normal torus S such that for some $k \geq 1$, the surface kS is a sum of good tori. These good tori must all be vertical. Moreover, if \mathcal{F} only contains one good vertical torus V , then V must be (up to isotopy) the only vertical essential torus in \mathcal{F} . \square

We start by discussing how to test whether e is isotopic to an exceptional fibre, since this is much easier than the regular case. If e is isotopic to an exceptional fibre, then observe that the triangulation \mathcal{D} is fibred over a disc with two exceptional fibres, which implies that \mathcal{D} contains a vertical annulus A that cuts \mathcal{D} into a pair of solid tori. Thus, if we can show that no such annulus A exists, then we will have certified that e is not isotopic to an exceptional fibre. This is the main idea behind the following algorithm (which is an important subroutine for our main algorithm):

Algorithm 12. *Let \mathcal{F} be a triangulation of an orientable irreducible 3-manifold with one torus boundary component (and no other boundary components). To test whether \mathcal{F} is fibred over a disc with two exceptional fibres:*

- (1) *Create an empty list \mathcal{A} .*
- (2) *Enumerate all vertex normal surfaces in \mathcal{F} . For each such surface S :*
 - *If S is an essential compressing disc, terminate and return `false`.*
 - *If S is an annulus, add S to \mathcal{A} .*
 - *If $2S$ is an annulus, add $2S$ to \mathcal{A} .*

(3) For each annulus S in \mathcal{A} , check whether cutting along S decomposes \mathcal{F} into a pair of solid tori. If there is an annulus that gives the desired decomposition, terminate and return `inconclusive`; otherwise, terminate and return `false`.

Proposition 13. *If Algorithm 12 returns `false`, then the input triangulation \mathcal{F} cannot have been fibred over a disc with two exceptional fibres.*

Proof. Suppose the input triangulation \mathcal{F} is fibred over a disc with two exceptional fibres. We need to prove that the algorithm will not return `false`. Since \mathcal{F} has incompressible boundary, it suffices to show that the algorithm will find an annulus of the desired type. Up to isotopy, the only essential annulus in \mathcal{F} is a vertical annulus A that cuts \mathcal{F} into a pair of solid tori. Proposition 11 tells us that A appears as either a vertex normal surface or the double of a vertex normal surface, and hence that the algorithm will return `inconclusive` in step (3). \square

We now discuss how to test whether e is isotopic to a regular fibre. If e is isotopic to a regular fibre, then observe that the triangulation \mathcal{D} is fibred over a disc with three exceptional fibres, which implies that \mathcal{D} has:

- exactly three vertical essential annuli, each of which separates one exceptional fibre from the other two, and therefore cuts \mathcal{D} into two pieces \mathcal{P}_0 and \mathcal{P}_1 , where \mathcal{P}_0 is a solid torus and \mathcal{P}_1 is fibred over a disc with two exceptional fibres; and
- exactly three vertical essential tori, each of which encloses two of the three exceptional fibres, and therefore cuts \mathcal{D} into two pieces \mathcal{Q}_0 and \mathcal{Q}_1 , where \mathcal{Q}_0 is fibred over an annulus with one exceptional fibre and \mathcal{Q}_1 is fibred over a disc with two exceptional fibres.

In particular, to rule out the existence of vertical essential tori in \mathcal{D} , we need to be able to recognise 3-manifolds \mathcal{M} that are fibred over an annulus with one exceptional fibre. For this, we rely on the fact that (up to isotopy) the only vertical essential annulus in such a 3-manifold \mathcal{M} is a vertical annulus that cuts \mathcal{M} into a single solid torus. With this in mind, the following algorithm is another important subroutine for our main algorithm:

Algorithm 14. *Let \mathcal{F} be a triangulation of an orientable irreducible 3-manifold with two torus boundary components (and no other boundary components). To test whether \mathcal{F} is fibred over an annulus with one exceptional fibre:*

- (1) Create an empty list \mathcal{A} .
- (2) Enumerate all vertex normal surfaces in \mathcal{F} . For each such surface S :
 - If S is an essential compressing disc, terminate and return `false`.
 - If S is an annulus, add S to \mathcal{A} .
 - If $2S$ is an annulus, add $2S$ to \mathcal{A} .
- (3) For each annulus S in \mathcal{A} , check whether cutting along S decomposes \mathcal{F} into a single solid torus. If there is an annulus that gives the desired decomposition, terminate and return `inconclusive`; otherwise, terminate and return `false`.

Proposition 15. *If Algorithm 14 returns `false`, then the input triangulation \mathcal{F} cannot have been fibred over an annulus with one exceptional fibre.*

Proof. Suppose the input triangulation \mathcal{F} is fibred over an annulus with one exceptional fibre. We need to prove that the algorithm will not return `false`. Since \mathcal{F} has incompressible boundary, it suffices to show that the algorithm will find an annulus of the desired type. As we already observed, up to isotopy, the only vertical essential annulus in \mathcal{F} is a vertical annulus A that cuts \mathcal{F} into a single solid torus. Proposition 11 tells us that A appears as either a vertex normal surface or the double of a vertex normal surface, and hence that the algorithm returns `inconclusive` in step (3). \square

With all this in mind, we are finally ready to present our main algorithm. We have already mentioned that the difficult case is testing whether e is isotopic to a regular fibre, and that in this case \mathcal{D} must have several vertical essential annuli and vertical essential tori. Thus, the overall strategy is similar to the previous two algorithms: use Proposition 11 to try to rule out the existence of these vertical essential surfaces.

Algorithm 16. Let \mathcal{T} be a one-vertex triangulation of an irreducible small Seifert fibre space that is neither a lens space nor a prism manifold. To test whether an edge e of \mathcal{T} is isotopic to a Seifert fibre:

- (1) Build a triangulation \mathcal{D} of the 3-manifold obtained by deleting a small solid torus neighbourhood of e .
- (2) Create empty lists \mathcal{A} , \mathcal{B} and \mathcal{L} .
- (3) Enumerate all vertex normal surfaces in \mathcal{D} . For each such surface S :
 - If S is an essential compressing disc, terminate and return `false`.
 - If S is an annulus, add S to \mathcal{A} .
 - If $2S$ is an annulus, add $2S$ to \mathcal{A} .
 - If S is a torus, add S to \mathcal{B} .
 - If $2S$ is a torus, add $2S$ to \mathcal{B} .
- (4) If the list \mathcal{A} is still empty, terminate and return `false`.
- (5) For each annulus S in \mathcal{A} :
 - (i) Cut along S , and check whether this yields two components \mathcal{C}_0 and \mathcal{C}_1 . If not, move on to the next annulus in \mathcal{A} .
 - (ii) Check whether \mathcal{C}_0 and \mathcal{C}_1 are solid tori.
 - If they are both solid tori, terminate and return `inconclusive`.
 - If \mathcal{C}_0 is a solid torus but \mathcal{C}_1 is not, add \mathcal{C}_1 to \mathcal{L} .
 - If \mathcal{C}_1 is a solid torus but \mathcal{C}_0 is not, add \mathcal{C}_0 to \mathcal{L} .
- (6) If the list \mathcal{B} contains fewer than two tori, terminate and return `false`.
- (7) Run Algorithm 12 on each triangulation \mathcal{P} in the list \mathcal{L} , and check whether the output is always `false`. If so, terminate and return `false`.
- (8) Initialise an integer variable n to be 0.
- (9) For each torus S in \mathcal{B} :
 - (i) Cut along S , and check whether this yields two components \mathcal{C}_0 and \mathcal{C}_1 . If not, move on to the next torus in \mathcal{B} .
 - (ii) Count the number b of boundary components in \mathcal{C}_0 .
 - In the case where $b = 1$, check that:
 - \mathcal{C}_1 has 2 boundary components;
 - running Algorithm 12 on \mathcal{C}_0 does not result in output `false`; and
 - running Algorithm 14 on \mathcal{C}_1 does not result in output `false`.
If these conditions are all satisfied, increase n by 1.
 - In the case where $b = 2$, check that:
 - \mathcal{C}_1 has 1 boundary component;
 - running Algorithm 14 on \mathcal{C}_0 does not result in output `false`; and
 - running Algorithm 12 on \mathcal{C}_1 does not result in output `false`.
If these conditions are all satisfied, increase n by 1.
- (10) If $n < 2$, terminate and return `false`; otherwise, terminate and return `inconclusive`.

Theorem 17. If Algorithm 16 returns `false`, then the edge e of interest cannot be isotopic to a Seifert fibre.

Proof. We first note that if e is isotopic to an exceptional fibre, then the triangulation \mathcal{D} will be fibred over a disc with two exceptional fibres. In this case, we can use the same argument as in the proof of Proposition 13 to show that Algorithm 16 will return `inconclusive` in step (5). (Note that in this case, \mathcal{D} has no essential tori, which is why we need to wait until step (6) to check whether the list \mathcal{B} contains at least two tori.)

Thus, for the rest of this proof, we assume that e is isotopic to a regular fibre, in which case \mathcal{D} is fibred over a disc with three exceptional fibres. In particular, \mathcal{D} will have incompressible boundary, so the algorithm will not return `false` in step (3).

To see that the algorithm will not return `false` in steps (4) and (7), we use the following fact (mentioned earlier): \mathcal{D} has exactly three vertical essential annuli, each of which cuts \mathcal{D} into a solid torus piece \mathcal{P}_0 and a piece \mathcal{P}_1 that is fibred over a disc with two exceptional fibres. By Proposition 11, at least one of these vertical annuli appears as either a vertex normal surface or the double of a vertex normal surface. Thus, at some point in step (3), we will add such an annulus S to the list \mathcal{A} , which

implies that the algorithm will not return `false` in step (4). Moreover, at some point in step (5), we will cut along S , and hence decompose \mathcal{D} into the pieces \mathcal{P}_0 and \mathcal{P}_1 mentioned earlier. The piece \mathcal{P}_1 will be added to the list \mathcal{L} , which means that at some point in step (7), we will run Algorithm 12 on input \mathcal{P}_1 ; by Proposition 13, Algorithm 12 cannot output `false` in this case, so our main algorithm also cannot return `false` at this point.

All that remains is to show that the algorithm will not return `false` in steps (6) and (10). For this, we use the following fact (also mentioned earlier): \mathcal{D} has exactly three vertical essential tori, each of which cuts \mathcal{D} into a piece \mathcal{Q}_0 that is fibred over an annulus with one exceptional fibre and a piece \mathcal{Q}_1 that is fibred over a disc with two exceptional fibres. By Proposition 11, at least two of these vertical tori appear as either vertex normal surfaces or doubles of vertex normal surfaces. Thus, at some point in step (3), we will add two such tori S_0 and S_1 to the list \mathcal{B} , which implies that the algorithm will not return `false` in step (6). Moreover, for each $i \in \{0, 1\}$, we will cut along S_i at some point in step (9), and hence decompose \mathcal{D} into the pieces \mathcal{Q}_0 and \mathcal{Q}_1 mentioned earlier. We subsequently run Algorithm 14 on \mathcal{Q}_0 and Algorithm 12 on \mathcal{Q}_1 ; by Propositions 15 and 13, respectively, neither of these subroutines will output `false`. Thus, we increment the variable n once for each $i \in \{0, 1\}$, which implies that our main algorithm cannot return `false` in step (10). \square

Implementations of algorithms 12, 14 and 16 are available at <https://github.com/AlexHe98/triang-counterex>. The only aspect of these implementations that we have not yet mentioned is that we include an alternative technique for testing whether a 3-manifold is Seifert fibred in a particular way, as this sometimes allows us to avoid the computationally expensive task of enumerating vertex normal surfaces. Specifically, each of our implementations begins by attempting combinatorial recognition: performing elementary moves (such as 2-3 and 3-2 moves) with the goal of obtaining a standard triangulation of a Seifert fibre space that is recognised by `Regina`'s `BlockedSFS` class [9].

3.3 Tracking edges as we perform 2-3 and 3-2 moves

Suppose that in some triangulation \mathcal{T} , we already know which edges are (for instance) core edges. Recall from section 2.2 that if we generate a new triangulation \mathcal{T}' by performing a 3-2 move about an edge e of \mathcal{T} , then the only difference between the 1-skeletons of \mathcal{T} and \mathcal{T}' is that \mathcal{T}' no longer contains the edge e . Thus, in principle, we do not need to directly compute which edges of \mathcal{T}' are core edges; we can just recover this information from what we already know about \mathcal{T} .

In the other direction, if we generate a new triangulation \mathcal{T}' by performing a 2-3 move, then recall that the only difference between the 1-skeletons of \mathcal{T} and \mathcal{T}' is that \mathcal{T}' contains a new edge e . In this case, we need to check whether e is a core edge, but there should be no need to recompute this for the other edges.

In practice, the situation is complicated by the fact that performing 2-3 and 3-2 moves in `Regina` could arbitrarily renumber the edges. Our solution is to use a bespoke implementation of 2-3 and 3-2 moves that provides, as part of the output, a description of how the edges are renumbered. The source code is available at <https://github.com/AlexHe98/triang-counterex>. This implementation—and more generally, this idea of tracking how an elementary move renames the vertices, edges or faces of a triangulation—may have other applications.

4 Removing “unwanted” edges using a targeted search

This section is devoted to discussing the main algorithm that we use to search for counterexamples to Conjectures 1, 2 and 3. We give an overview of the algorithm in sections 4.1 and 4.2, and then discuss various implementation details in sections 4.3 and 4.4.

4.1 The degree defect and the multiplicity defect

As mentioned in section 1.2, a natural way to remove an “unwanted” edge e is to perform a 3-2 move about e . Such a move is possible if and only if e has degree three and actually meets three distinct tetrahedra. This motivates the following definitions:

Definitions 18. Let e be an edge in a one-vertex triangulation. Let $d(e)$ denote the degree of e , and let $n(e)$ denote the number of *distinct* tetrahedra that meet e .

- The **degree defect** of e , denoted $\delta(e)$, is given by $|d(e) - 3|$.
- The **multiplicity defect** of e , denoted $\mu(e)$, is given by $d(e) - n(e)$.

Note that the degree defect and multiplicity defect are both always non-negative, and that we can perform a 3-2 move about an edge e if and only if both of these defects are equal to zero. This gives us an obvious objective: minimise these two defects for all unwanted edges. Crucially, this means that instead of enumerating potential counterexamples by brute force—which quickly becomes computationally infeasible because (for a fixed 3-manifold) the number of possible triangulations increases at least exponentially as we increase the size—we can enumerate triangulations in a targeted fashion, by greedily prioritising triangulations in which the unwanted edges have small degree defect and multiplicity defect. To make this idea precise, we begin with the following definition:

Definition 19 (Complexity of a triangulation). Let \mathcal{T} be a one-vertex triangulation, and consider a collection $\{e_1, \dots, e_k\}$ of “unwanted” edges in \mathcal{T} , where $k \geq 1$. The **complexity** of \mathcal{T} (with respect to the “unwanted” edges) is given by the 4-tuple

$$\left(k, \max_{1 \leq i \leq k} \mu(e_i), \max_{1 \leq i \leq k} \delta(e_i), |\mathcal{T}| \right).$$

Our goal is to minimise the complexity of a triangulation with respect to the *lexicographical ordering*. This is why the number k of “unwanted” edges appears as the first entry: depending on context, the “unwanted” edges may be the core edges, the tunnel edges or the edges isotopic to Seifert fibres, and our primary objective is to reduce the number of these edges.

Our secondary objective, as we have already discussed, is to reduce the multiplicity defect and degree defect of the “unwanted” edges, in the hope that this will allow us to remove these edges using 3-2 moves. We take the maximum defects across all “unwanted” edges (as opposed to, say, the minimum) because our ultimate goal is to remove all of these edges, not just one of them.

It is crucial that we prioritise reducing the multiplicity defect ahead of reducing the degree defect. The reason for this is best illustrated by recounting our initial approach to this problem. At first, our complexity did not involve the multiplicity defect at all. With this naïve notion of complexity, we found that the search could easily reach a region of the Pachner graph where the “unwanted” edges had degree defect close to 0. However, the search would then get stuck enumerating lots of triangulations without ever actually reducing the degree defect to 0. We eventually realised that the search was getting trapped in a region of the Pachner graph where the “unwanted” edges had multiplicity defect equal to 2. Placing a high priority on reducing the multiplicity defect gives the search some impetus to avoid such regions.

Finally, all else being equal, it would be nice for our counterexamples to be as small as possible. Thus, we include the size of the triangulation as the final entry of the complexity.

4.2 The targeted search algorithm

Algorithm 20. In a one-vertex triangulation, let P be a property of edges that is invariant under ambient isotopy. Call an edge **bad** if it satisfies property P , and **good** otherwise. This algorithm takes the following inputs:

- A one-vertex triangulation \mathcal{T} with n bad edges, where $n \geq 1$.
- A non-negative integer x (the number of extra bad edges that we are allowed to use).

To search for a new triangulation with $n - 1$ bad edges:

- (1) For each bad edge in \mathcal{T} , check whether it is possible to perform a 3-2 move about this edge. If such a move is possible, terminate and return the triangulation that results from performing this move.
- (2) Create a set \mathcal{S} . Also create a priority queue \mathcal{Q} that stores triangulations in order of increasing complexity (with respect to the bad edges). Add \mathcal{T} to both \mathcal{S} and \mathcal{Q} .
- (3) While \mathcal{Q} is non-empty:

- (i) Remove the first triangulation \mathcal{F} (i.e., a triangulation with smallest complexity) from \mathcal{Q} , and let m denote the number of bad edges in \mathcal{F} .
- (ii) Call a 3-2 move about an edge e **eligible** if e is a good edge; for a 2-3 move, let e denote the new edge that is created by this move, and call this move **eligible** if either e is a good edge, or e is a bad edge but $m < n + x$. For each eligible move on \mathcal{F} , check whether (up to combinatorial isomorphism) the set \mathcal{S} already contains the triangulation \mathcal{G} that we obtain after performing this move. If not:
 - Add \mathcal{G} to both \mathcal{S} and \mathcal{Q} .
 - Perform all possible sequences of 3-2 moves about bad edges in \mathcal{G} . For each triangulation \mathcal{T}' that we obtain from such moves, if \mathcal{T}' does not already appear in the set \mathcal{S} (up to combinatorial isomorphism), then add \mathcal{T}' to both \mathcal{S} and \mathcal{Q} .
 - If we can find such a sequence consisting of $m - n + 1$ 3-2 moves, then the final triangulation \mathcal{T}^* in this sequence has $n - 1$ bad edges. Terminate and return \mathcal{T}^* .

Visit <https://github.com/AlexHe98/triang-counterex> to see an implementation of this algorithm. We discuss the major details of this implementation in sections 4.3 and 4.4.

It is worthwhile to explain why we terminate the search as soon as we find a triangulation with $n - 1$ bad edges, rather than allowing the search to continue until it (hopefully) finds a triangulation with no bad edges at all. This is partly a remnant of our early investigations into the conjectures from section 1.1; initially, it was not at all clear whether (for instance) triangulations with no core edges even existed, so we were happy to make any kind of progress towards reducing the number of core edges. One reason we have persisted with terminating the search early is that we have, on occasion, found it useful to have the flexibility to make adjustments as we progressively lower the number of bad edges. Examples of such adjustments include:

- changing the number x of extra bad edges that we allow Algorithm 20 to use (though we have not encountered an example where this particular adjustment was helpful);
- changing the number of concurrent processes that we use in step (3) of Algorithm 20 (we discuss this in more detail in section 4.3, and give examples in section 5.1 and appendix B); or
- even changing how we measure the complexity of a triangulation (see section 5.3 for an example where this was useful).

4.3 Troublesome regions, concurrent computation, and instability

In section 4.1, we mentioned regions of the Pachner graph where the “unwanted” edges have very low degree defect, but multiplicity defect equal to 2 (such edges naturally occur, for instance, at the hearts of layered solid tori). Although placing a high priority on reducing multiplicity defect does help the search avoid such regions, if the search nevertheless gets trapped in such a region then it can be quite difficult to escape because the only way out is to perform moves that *increase* the degree defect of the “unwanted” edges.

This phenomenon occurs more generally: a locally optimal move can send the search into a “troublesome” region (which could, a priori, be *infinite*) of the Pachner graph where none of the subsequently available moves decrease the complexity of the triangulation. In the case discussed above, this causes the search to get stuck enumerating lots of triangulations with similar complexity; as we will see in section 5.1, there are also cases where the search can start enumerating lots of triangulations with *rapidly increasing* complexity.

Algorithm 20 is especially vulnerable to falling into such troublesome regions if we deal with triangulations one at a time in step (3). However, when we instead use multiple processes to deal with several triangulations concurrently, the search is sometimes able to either avoid or escape these troublesome regions. There are probably two drivers for this:

- (1) using multiple processes causes the search to explore with more “breadth” than a purely greedy approach, and
- (2) the search gains some randomness because the order in which triangulations are inserted into the priority queue \mathcal{Q} could vary each time we run the search.

There may be more direct methods to achieve similar behaviour; our method was good enough, and had a low cost (both in human effort and in computational complexity).

One drawback is that it is impossible to know in advance how many concurrent processes we should use. In fact, as we will see in section 5, there is often a “sweet spot” where running the search will produce a triangulation \mathcal{T}^* with the desired number of bad edges, but if we significantly increase or decrease the number of processes, then the search tends to get trapped in a troublesome region.

Our solution is to implement Algorithm 20 so that it periodically prints an update on the complexity of the triangulations that it is currently dealing with, and to manually check that the search is making satisfactory progress towards reducing the complexity. If we do not observe such progress, then we simply restart the search, possibly with a change to the number of concurrent processes that we use. Although it is not ideal that some human intervention is required, this is not unheard of for difficult problems in computational topology that only need to be successfully solved once (such as finding a counterexample). Another example of this is the work done in [8] to extend the census of prime knots up to 19 crossings.

The last thing that we mention in this section is that our implementation is quite unstable. Indeed, we have already noted that the search can produce different results when we use a different number of concurrent processes, or when we simply rerun the search. We have encountered one other manifestation of this instability: refactoring the source code can drastically change the behaviour of the search. We have not managed to find a way to modify the algorithm to make it more stable.

4.4 Other implementation details

We now outline some other important details of our implementation of Algorithm 20.

First, as mentioned in section 3.3, we use a bespoke implementation of 2-3 and 3-2 moves which allows us to minimise how often we need to check whether an edge is bad. This is crucial because for our purposes, checking whether an edge is bad generally relies on computationally expensive techniques involving normal surfaces:

- To recognise core edges and tunnel edges, we need to be able to recognise solid tori and genus-2 handlebodies, respectively. These are both special cases of handlebody recognition (Algorithm 9).
- To recognise edges isotopic to Seifert fibres, we rely on Algorithm 16.

Second, since Algorithm 20 always considers triangulations up to combinatorial isomorphism, we actually store isomorphism signatures in the set \mathcal{S} and the priority queue \mathcal{Q} . As described in [5], isomorphism signatures are a standard and indispensable tool when exploring the Pachner graph.

Third, when the priority queue \mathcal{Q} contains multiple triangulations with the same complexity, we choose to prioritise such triangulations by insertion order.

Finally, in practice, we usually set the input variable x to be 0, in which case Algorithm 20 discards all triangulations with more bad edges than the input triangulation \mathcal{T} . Having said this, there are occasions where taking $x > 0$ —and hence allowing the number of bad edges to increase—may be beneficial; we discuss this in a little more detail in section 5.3.

5 The counterexamples

In sections 5.1, 5.2 and 5.3, we discuss experimental details specific to each of the three conjectures stated in section 1.1. As mentioned in section 1, we give counterexamples to all three of these conjectures. Moreover, we show in section 5.4 that each of our counterexamples can be turned into an infinite family of counterexamples.

All of the computations that we discuss in this section were run on a laptop with an Intel Core i5-7200U processor, which has just two physical cores divided into four logical processors. It is therefore remarkable that we were able to obtain almost all of our counterexamples in no more than a few *minutes* of wall time; even the worst example that we present (see Figure 28 in appendix B) required less than 34 minutes of wall time. This is mostly due to the fact that our targeted search was able to home in on an extremely small portion of the search space: for each 3-manifold for which we successfully found a counterexample, we never needed to enumerate more than a few thousand triangulations.

5.1 Triangulations with no core edges

We first discuss the special case of the 3-sphere; in this case, core edges are equivalent to *unknotted edges*. We saw in section 1.2 that the 3-sphere has 422 533 279 one-vertex triangulations with 10 or fewer tetrahedra, and that all of these triangulations have a core edge (in fact, at least two core edges). In spite of this seemingly compelling evidence, the triangulation \mathcal{T} with isomorphism signature

```
uLLvQQvLAPvPAQccdfeghhgmklrnorsqsstthsaaagggaaaaanaaagb
```

turns out to be a 20-tetrahedron one-vertex 3-sphere with no core edges.

To find this counterexample, we began by arbitrarily selecting the triangulation \mathcal{T}_2 with isomorphism signature `cMcabbgqs`; this is a one-vertex 3-sphere with complexity $(2, 5, 4, 2)$ (recall Definition 19). After running Algorithm 20 twice, we obtained a 22-tetrahedron one-vertex triangulation \mathcal{T}_0 of the 3-sphere with no core edges; the results are summarised in Figure 7.

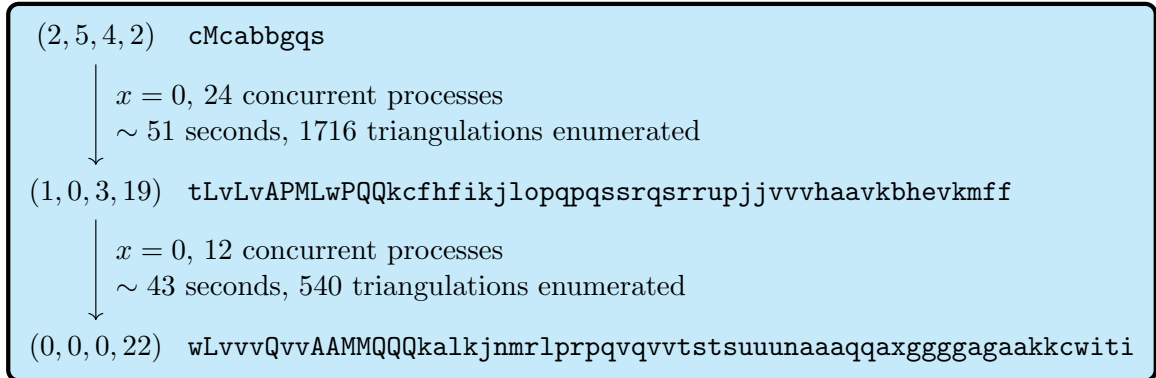


Figure 7: Removing core edges from `cMcabbgqs` (3-sphere).

To turn \mathcal{T}_0 into the 20-tetrahedron example \mathcal{T} , we ran a breadth-first search through the Pachner graph, but with the restriction that we ignored any 2-3 move that introduces a core edge. This took approximately 367 seconds of wall time. We also know that we cannot reduce the size further (still ignoring 2-3 moves that introduce core edges) without passing through at least one triangulation with more than 23 tetrahedra; checking this required an additional 228 seconds of wall time.

It is worth noting that to remove one core edge from \mathcal{T}_2 , we tried running Algorithm 20 with different numbers of concurrent processes, but using 24 processes seems to produce the best results. In particular, we initially tried using 12 processes, but this produced a triangulation with isomorphism signature

```
sLvAAvLAzMMQQcdcef1kmjmqonprqprrhvrvqnkkksqeeekocksf
```

and complexity $(1, 2, 1, 18)$. The core edge in this triangulation has multiplicity defect 2 but degree defect 1; this is exactly one of the troublesome cases that we mentioned in section 4.3. We needed to increase the number of processes to 24 to avoid this.

Somewhat surprisingly, increasing the number of processes significantly beyond 24 also appears to have an adverse affect on the effectiveness of Algorithm 20. For example, with 36 processes, although the search is sometimes able to remove a core edge, it seems to do so less reliably. Instead, we find that the search has a tendency to get trapped in a different type of troublesome region:

- After about 10 seconds, the search reaches a triangulation with complexity $(2, 4, 16, 15)$.
- After about 20 seconds, the search reaches a triangulation with complexity $(2, 4, 23, 22)$.
- After about 30 seconds, the search reaches a triangulation with complexity $(2, 4, 26, 25)$.

When this happens, the complexity only appears to increase further if we allow the search to continue.

We finish this section by mentioning that we also found triangulations with no core edges for the following lens spaces: $L_{6,1}$, $L_{9,2}$, $L_{11,2}$, $L_{13,3}$, and $L_{16,3}$. See appendix A for detailed results.

5.2 Triangulations with no tunnel edges

All fourteen prime knots with crossing number up to 7 have tunnel number equal to one. Except for the 5_2 knot, we were able to find ideal triangulations with no tunnel edges for all of these knots:

- For the trefoil knot (also known as the 3_1 knot), we arbitrarily selected the isomorphism signature $cPcbbbadu$. Figure 8 summarises the result of running Algorithm 20.

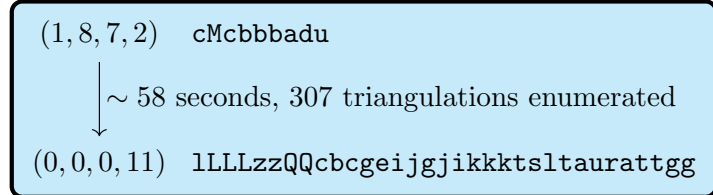


Figure 8: Removing tunnel edges from $cPcbbbadu$ (trefoil knot); $x = 0, 8$ processes.

- For the figure-eight knot (also known as the 4_1 knot), we arbitrarily selected the isomorphism signature $cPcbbbiht$. Figure 9 summarises the results of running Algorithm 20 twice.

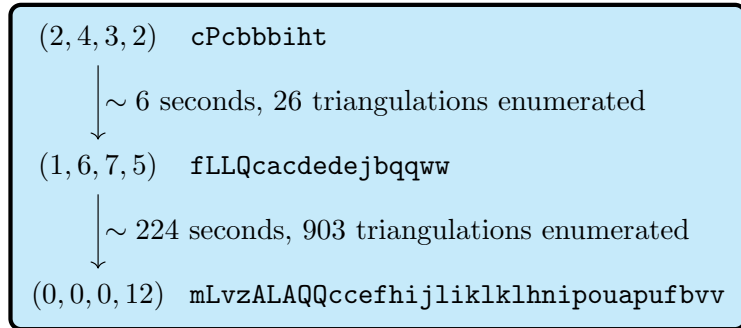


Figure 9: Removing tunnel edges from $cPcbbbiht$ (figure-eight knot); $x = 0, 24$ processes.

- For the $(5, 2)$ torus knot (also known as the 5_1 knot), we arbitrarily selected the isomorphism signature $dLQbcccaekv$. Figure 10 summarises the results of running Algorithm 20 twice.

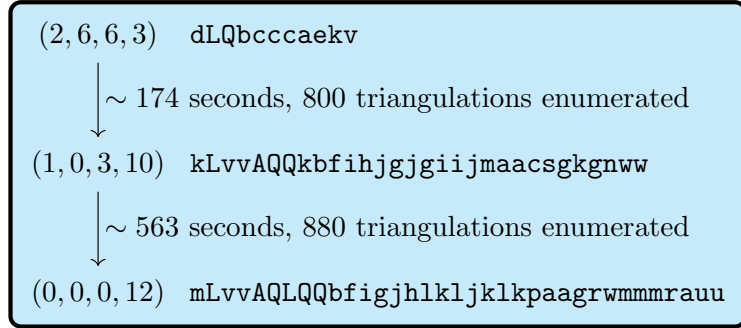


Figure 10: Removing tunnel edges from $dLQbcccaekv$ $((5, 2)$ torus knot); $x = 0, 24$ processes.

- We also found triangulations with no tunnel edges for all ten prime knots with crossing number equal to 6 or 7. See appendix B for detailed results.

One striking observation is that although the triangulations here are relatively small, and although we only enumerated relatively few triangulations, our running times are nevertheless significantly longer than those in section 5.1. The main reason for this is probably that recognising genus-2 handlebodies is more expensive than recognising solid tori.

5.3 Triangulations with no edges isotopic to Seifert fibres

Let \mathcal{M} denote the small Seifert fibre space $\mathcal{S}(\frac{1}{2}, \frac{2}{3}, -\frac{1}{3})$ (recall Construction 5). We found the following 11-tetrahedron one-vertex triangulation \mathcal{T} of \mathcal{M} , which turns out to have no edges isotopic to Seifert fibres:

`1LLLLPMQccddfjiihikkpkrvaaacttvc.`

To do this, we began with the isomorphism signature `fLLQcaceeedjkuxkj`. Running Algorithm 20 four times with $x = 1$ and 12 concurrent processes produced a 13-tetrahedron triangulation \mathcal{T}^* with no edges isotopic to Seifert fibres; the results are summarised in Figure 11. We then used a breadth-first search (similar to the one from section 5.1) to turn \mathcal{T}^* into the 11-tetrahedron triangulation \mathcal{T} .

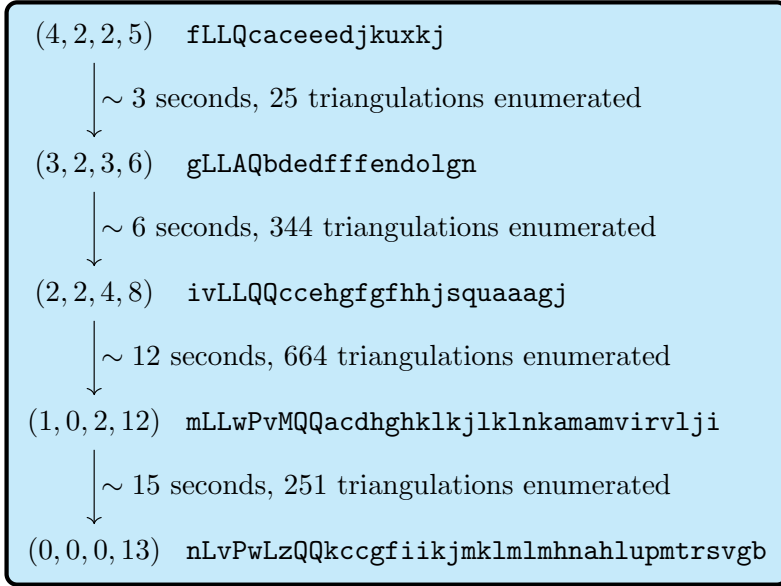


Figure 11: Removing edges isotopic to Seifert fibres from `fLLQcaceeedjkuxkj` ($\mathcal{M} = \mathcal{S}(\frac{1}{2}, \frac{2}{3}, -\frac{1}{3})$); $x = 1$, 12 processes.

The reason for taking $x = 1$ instead of $x = 0$ comes from older versions of the code. Early versions of Algorithm 16 included fewer normal surfaces in the analysis, making it less effective at identifying good edges (in this context, edges not isotopic to Seifert fibres). At the time, we encountered triangulations that were “dead ends”, in the following sense: every 2-3 move would create an edge that we could not certify as good. Our short-term solution was to allow the search to introduce extra bad edges if necessary. Having since strengthened Algorithm 16, taking $x = 1$ no longer seems necessary for the example that we just discussed; we did not revert to using $x = 0$ simply because we found no compelling reason to do so.

It is also worth mentioning that we encountered one example where even taking $x = 1$ was not enough to prevent “dead ends” (even with the current implementation of Algorithm 16). Specifically, this happens for the triangulation with isomorphism signature `fvPQcdecedekrsnrs` and complexity $(6, 0, 2, 5)$; this represents the *Poincaré homology sphere*, which admits the Seifert fibration $\mathcal{S}(\frac{1}{2}, \frac{1}{3}, -\frac{4}{5})$. When we increased the value of x to 2, we were able to reach a triangulation with four edges isotopic to Seifert fibres, but we did not make any further progress.

On a related note, we did manage to find a counterexample for one other small Seifert fibre space, namely $\mathcal{S}(\frac{1}{2}, \frac{1}{3}, \frac{2}{3})$, which we denote by \mathcal{M}' . Specifically, we found the following 20-tetrahedron triangulation \mathcal{T}' of \mathcal{M}' , which has no edges isotopic to Seifert fibres:

`uLLPvvLQLAPAPQccdfeknlipnomqnrtstssthspaaaliaravlkuaaxxxx.`

To do this, we began with the isomorphism signature `gLLMQacdefefjkaknkr`, which has complexity $(4, 2, 4, 6)$. However, we were not able to remove all four edges isotopic to Seifert fibres by simply running Algorithm 20 four times. Instead, to remove the first and third such edges, we needed to modify how our search measured the complexity of our triangulations.

To describe this modification, consider a one-vertex triangulation \mathcal{S} of \mathcal{M}' , and let e_1, \dots, e_k denote all the bad edges in \mathcal{S} (where, ‘‘bad’’ in this context means that the edge is isotopic to a Seifert fibre). We should imagine that \mathcal{S} is some intermediate triangulation that we encounter in a search similar to Algorithm 20, so in the background there is some initial input triangulation that has n bad edges, and there is also some non-negative integer x such that the search discards any triangulations with more than $n + x$ bad edges. However, unlike in Algorithm 20, we temporarily forget about needing to remove all k bad edges in \mathcal{S} , and instead focus entirely on the intermediate goal of removing $k - n + 1$ bad edges from \mathcal{S} (and hence reducing the number of bad edges to $n - 1$). To this end, we single out two (not necessarily distinct) bad edges as follows:

- Arrange the bad edges in order of increasing *multiplicity defect*, and take e_m to be the $(k - n + 1)$ st bad edge in this ordering.
- Arrange the bad edges in order of increasing *degree defect*, and take e_d to be the $(k - n + 1)$ st bad edge in this ordering.

We modify Algorithm 20 by measuring the complexity of \mathcal{S} as follows:

$$(k, \mu(e_m), \delta(e_d), |\mathcal{S}|).$$

Figure 12 summarises the results of removing all four edges isotopic to Seifert fibres from the triangulation of \mathcal{M}' given by the isomorphism signature $\text{gLLM}\text{Qacdefefjkaknkr}$; we used $x = 1$ and 12 concurrent processes at each stage, and in the stages where we used the modified complexity we list the (unmodified) complexity above the modified complexity. We obtained a 25-tetrahedron triangulation of \mathcal{M}' with no edges isotopic to Seifert fibres, which we then simplified to the 20-tetrahedron triangulation \mathcal{T}' using the same breadth-first search technique as before.



Figure 12: Removing edges isotopic to Seifert fibres from $\text{gLLM}\text{Qacdefefjkaknkr}$ ($\mathcal{M}' = \mathcal{S}(\frac{1}{2}, \frac{1}{3}, \frac{2}{3})$); $x = 1, 12$ processes. The boxes indicate where we used the modified complexity.

5.4 From one counterexample to infinitely many

Here, we show that each of the above counterexamples can be turned into infinite families. The key is the following proposition:

Proposition 21. *Let \mathcal{M} be either a closed 3-manifold, or a 3-manifold with a single boundary component of positive genus (and no other boundary components). In the closed case, let \mathcal{T} be a one-vertex triangulation of \mathcal{M} ; in the bounded case, let \mathcal{T} be a one-vertex ideal triangulation of \mathcal{M} . Let P be a property of edges of \mathcal{T} that is invariant under ambient isotopy. Call \mathcal{T} **interesting** if every edge in \mathcal{T} satisfies P . If \mathcal{M} has an interesting triangulation, then \mathcal{M} has infinitely many interesting triangulations.*

Proof. Let \mathcal{T} be an interesting triangulation of \mathcal{M} . Fix a tetrahedron Δ of \mathcal{T} , and let e and f denote a pair of opposite edges of Δ . We obtain a new triangulation \mathcal{T}' of \mathcal{M} by replacing Δ with a three-tetrahedron gadget, as shown in Figure 13.¹³ In terms of 1-skeletons, observe that all we have done is introduce two new edges e' and f' such that e' is isotopic to e and f' is isotopic to f . Thus, \mathcal{T}' is an interesting triangulation of \mathcal{M} . Repeating this procedure indefinitely gives the desired infinite family of interesting triangulations of \mathcal{M} . \square

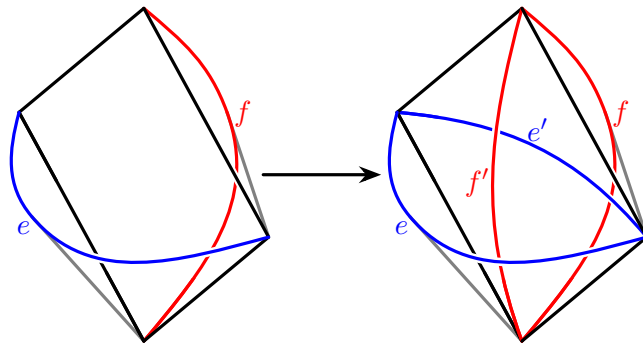


Figure 13: Building a new interesting triangulation.

Combining Proposition 21 with the counterexamples from sections 5.1, 5.2 and 5.3 immediately yields the following three theorems:

Theorem 22. *Let \mathcal{M} be one of the following lens spaces: the 3-sphere, $L_{6,1}$, $L_{9,2}$, $L_{11,2}$, $L_{13,3}$, or $L_{16,3}$. Then \mathcal{M} has infinitely many one-vertex triangulations with no core edges.*

Theorem 23. *Let K be a prime knot whose crossing number is at most 7, other than the 5_2 knot. Then K has infinitely many ideal triangulations with no tunnel edges.*

Theorem 24. *The small Seifert fibre spaces $\mathcal{S}(\frac{1}{2}, \frac{2}{3}, -\frac{1}{3})$ and $\mathcal{S}(\frac{1}{2}, \frac{1}{3}, \frac{2}{3})$ each have infinitely many one-vertex triangulations with no edges isotopic to Seifert fibres.*

6 Discussion

6.1 Unanswered questions

Although our targeted search allowed us to produce triangulations with no core edges for six different lens spaces, this did not work for all of the lens spaces that we tried. For reference, we failed to find counterexamples for the following lens spaces: $S^2 \times S^1$, $\mathbb{R}P^3$, $L_{3,1}$, $L_{5,1}$, $L_{7,2}$, $L_{8,3}$, $L_{10,3}$, $L_{11,3}$, $L_{12,5}$, $L_{13,5}$, $L_{7,1}$, $L_{14,3}$, $L_{15,4}$, $L_{16,7}$, $L_{17,5}$, $L_{18,5}$, $L_{19,7}$, $L_{21,8}$, $L_{8,1}$, and $L_{13,2}$. We nevertheless suspect that such counterexamples exist. Moreover, since we currently have no strong reason to believe otherwise, we tentatively propose the following conjecture:

Conjecture 25. *Every lens space admits infinitely many one-vertex triangulations with no core edges.*

For our other two problems of interest, our targeted search was again not always successful. As mentioned in section 5.2, we were not able to find an ideal triangulation of the 5_2 knot (which has tunnel number equal to one) with no tunnel edges. We also failed to find triangulations with no edges isotopic to Seifert fibres for the following small Seifert fibre spaces: $\mathcal{S}(\frac{1}{2}, \frac{1}{3}, -\frac{2}{3})$, $\mathcal{S}(\frac{1}{2}, \frac{1}{3}, -\frac{1}{3})$, $\mathcal{S}(\frac{1}{2}, \frac{1}{3}, -\frac{3}{4})$, $\mathcal{S}(\frac{1}{2}, \frac{1}{3}, -\frac{4}{5})$, and $\mathcal{S}(\frac{1}{2}, \frac{1}{3}, \frac{1}{3})$. Despite this, we propose the following conjecture:

¹³This modification is a special case of an elementary move known as a **0-2 move** or **lune move**.

Conjecture 26. *Every knot with tunnel number one admits infinitely many ideal triangulations with no tunnel edges.*

Conjecture 27. *For every small Seifert fibre space that is not a lens space or prism manifold, there exist infinitely many one-vertex triangulations with no edges isotopic to Seifert fibres.*

6.2 Future applications

Elementary moves such as 2-3 and 3-2 moves have many computational applications beyond how we used them in this paper. The two most common are:

- (1) using elementary moves to improve a triangulation, which is often critical for making exponential-time computations feasible; and
- (2) finding a sequence of moves that transforms a triangulation \mathcal{T} into another triangulation \mathcal{T}' , which gives a computational proof that \mathcal{T} and \mathcal{T}' are homeomorphic.

Finding the right sequence of moves can be difficult, so a targeted search could also be useful in these other settings.

In particular, increasing the number of tetrahedra is sometimes unavoidable [5]:

- (1) There are many triangulations \mathcal{T} of the 3-sphere such that to simplify \mathcal{T} to a smallest-possible triangulation via 2-3 and 3-2 moves, we must visit at least one intermediate triangulation with two more tetrahedra than \mathcal{T} . There is also a triangulation of a graph manifold for which simplification requires *three* additional tetrahedra.
- (2) In the census of minimal triangulations with up to 9 tetrahedra, there are many 3-manifolds for which two additional tetrahedra are required to find sequences of 2-3 and 3-2 moves that connect all pairs of minimal triangulations. There is also one 3-manifold—the lens space $L_{3,1}$ —for which *three* additional tetrahedra are required to connect all the minimal triangulations.

There are also situations where we might actually *want* to increase the number of tetrahedra, provided this improves the triangulation with respect to another quantity. One such quantity is the *treewidth*, which is important because some algorithms in 3-manifold topology are known to be fixed-parameter tractable in the treewidth [10, 12]. For such algorithms, the benefit of reducing the treewidth significantly outweighs the cost that would arise from increasing the number of tetrahedra. This has practical relevance because, as observed by Huszár and Spreer [17, Corollary 20], minimal triangulations (which minimise the number of tetrahedra) do not necessarily minimise the treewidth; here, we mention two examples of this, the first of which was given by Huszár and Spreer in [17]:

- Let \mathcal{M} denote the Poincaré homology sphere; as mentioned in section 5.3, \mathcal{M} admits the Seifert fibration $\mathcal{S}(\frac{1}{2}, \frac{1}{3}, -\frac{4}{5})$. The unique minimal triangulation for \mathcal{M} is given by the isomorphism signature `fvPQcdecedekeksnrs`; this is a 5-tetrahedron triangulation with treewidth 4. However, the isomorphism signature `hLALAkcbbeffggqqnmxkk` gives a 7-tetrahedron triangulation of \mathcal{M} with treewidth 2.
- In section 1, we mentioned that there is a Seifert fibre space—to be precise, the fibration is given by $\mathcal{S}(\frac{1}{2}, \frac{1}{3}, -\frac{9}{11})$ —whose unique minimal triangulation is given by the isomorphism signature `iLLLPQcbcggffghhtsmhgoso`; this is an 8-tetrahedron triangulation with treewidth 4. However, the standard prism-and-layering construction gives a 9-tetrahedron triangulation with treewidth 2; for completeness, the isomorphism signature is `jLAMLLQbcdbdeghhiixxnxxjqisj`.

The main takeaway from this discussion is that sometimes we might either want or need to increase the number of tetrahedra. As mentioned in section 1, increasing the number of tetrahedra is accompanied by a super-exponential increase in the number of triangulations; even if we fix a 3-manifold, this is still at least exponential (whether this is actually super-exponential remains open). This means that exhaustive search techniques quickly run into problems with not only running time, but also (often more importantly) memory management. However, our work in this paper suggests that, with the right heuristics, we may be able to circumvent these problems; the (still unresolved) challenge is to actually devise such heuristics in the settings mentioned above.

References

- [1] Gennaro Amendola. A calculus for ideal triangulations of three-manifolds with embedded arcs. *Math. Nachr.*, 278(9):975–994, 2005. doi:10.1002/mana.200310285.
- [2] David Bremner and Lars Schewe. Edge-graph diameter bounds for convex polytopes with few facets. *Experiment. Math.*, 20(3):229–237, 2011. doi:10.1080/10586458.2011.564965.
- [3] E. J. Brody. The topological classification of the lens spaces. *Ann. Math.*, 71(1):163–184, 1960. doi:10.2307/1969884.
- [4] Benjamin A. Burton. Detecting genus in vertex links for the fast enumeration of 3-manifold triangulations. In *Proceedings of the 36th International Symposium on Symbolic and Algebraic Computation*, pages 59–66. Association for Computing Machinery, 2011. doi:10.1145/1993886.1993901.
- [5] Benjamin A. Burton. Simplification paths in the Pachner graphs of closed orientable 3-manifold triangulations. [arXiv:1110.6080](https://arxiv.org/abs/1110.6080), 2011.
- [6] Benjamin A. Burton. Computational topology with Regina: Algorithms, heuristics and implementations. In *Geometry and Topology Down Under*, volume 597 of *Contemporary Mathematics*, pages 195–224. American Mathematical Society, 2013. doi:10.1090/conm/597.
- [7] Benjamin A. Burton. A new approach to crushing 3-manifold triangulations. *Discrete Comput. Geom.*, 52:116–139, 2014. doi:10.1007/s00454-014-9572-y.
- [8] Benjamin A. Burton. The Next 350 Million Knots. In Sergio Cabello and Danny Z. Chen, editors, *36th International Symposium on Computational Geometry (SoCG 2020)*, volume 164 of *Leibniz International Proceedings in Informatics (LIPIcs)*, pages 25:1–25:17. Schloss Dagstuhl–Leibniz-Zentrum für Informatik, 2020. URL: <https://drops.dagstuhl.de/opus/volltexte/2020/12183>, doi:10.4230/LIPIcs.SoCG.2020.25.
- [9] Benjamin A. Burton, Ryan Budney, William Pettersson, et al. Regina: Software for low-dimensional topology. <https://regina-normal.github.io>, 1999–2022.
- [10] Benjamin A. Burton, Clément Maria, and Jonathan Spreer. Algorithms and complexity for Turaev-Viro invariants. *Journal of Applied and Computational Topology*, 2:33–53, 2018. doi:10.1007/s41468-018-0016-2.
- [11] Benjamin A. Burton and Melih Özlen. A fast branching algorithm for unknot recognition with experimental polynomial-time behaviour. [arXiv:1211.1079](https://arxiv.org/abs/1211.1079), 2012. To appear in *Math. Program.*
- [12] Benjamin A. Burton and Jonathan Spreer. The complexity of detecting taut angle structures on triangulations. In *Proceedings of the 2013 Annual ACM-SIAM Symposium on Discrete Algorithms (SODA)*, pages 168–183. Society for Industrial and Applied Mathematics, 2013. doi:10.1137/1.9781611973105.13.
- [13] Marc Culler, Nathan M. Dunfield, Matthias Goerner, and Jeffrey R. Weeks. SnapPy, a computer program for studying the geometry and topology of 3-manifolds. Available at <http://snappy.computop.org> (14/08/2022).
- [14] Wolfgang Haken. Theorie der Normalflächen. *Acta Math.*, 105:245–375, 1961. doi:10.1007/BF02559591.
- [15] Joel Hass, Jeffrey C. Lagarias, and Nicholas Pippenger. The computational complexity of knot and link problems. *J. ACM*, 46(2):185–211, 1999. doi:10.1145/301970.301971.
- [16] Allen Hatcher. Notes on Basic 3-Manifold Topology. <https://pi.math.cornell.edu/~hatcher/3M/3Mfds.pdf>, 2007.

[17] Kristóf Huszár and Jonathan Spreer. 3-Manifold Triangulations with Small Treewidth. In Gill Barequet and Yusu Wang, editors, *35th International Symposium on Computational Geometry (SoCG 2019)*, volume 129 of *Leibniz International Proceedings in Informatics (LIPIcs)*, pages 44:1–44:20. Schloss Dagstuhl–Leibniz-Zentrum fuer Informatik, 2019. URL: <http://drops.dagstuhl.de/opus/volltexte/2019/10448>, doi:10.4230/LIPIcs.SOCG.2019.44.

[18] William Jaco and J. Hyam Rubinstein. 0-efficient triangulations of 3-manifolds. *J. Differential Geom.*, 65:61–168, 2003. doi:10.4310/jdg/1090503053.

[19] William Jaco and Peter B. Shalen. A new decomposition theorem for irreducible sufficiently large 3-manifolds. In R. James Milgram, editor, *Algebraic and Geometric Topology, Part 2*, volume XXXII of *Proceedings of Symposia in Pure Mathematics*, pages 71–84. American Mathematical Society, 1978. doi:10.1090/pspum/032.2.

[20] William Jaco and Jeffrey L. Tollefson. Algorithms for the complete decomposition of a closed 3-manifold. *Illinois J. Math.*, 39(3):358–406, 1995. doi:10.1215/ijm/1255986385.

[21] Klaus Johannson. *Homotopy Equivalences of 3-Manifolds with Boundaries*, volume 761 of *Lecture Notes in Mathematics*. Springer-Verlag, 1979. doi:10.1007/BFb0085406.

[22] Victor Klee. Paths on polyhedra. II. *Pacific J. Math.*, 17(2):249–262, 1966. doi:10.2140/pjm.1966.17.249.

[23] Marc Lackenby and Saul Schleimer. Recognising elliptic manifolds. [arXiv:2205.08802](https://arxiv.org/abs/2205.08802), 2022.

[24] Tao Li. An algorithm to find vertical tori in small Seifert fiber spaces. *Comment. Math. Helv.*, 81(4):727–753, 2006. doi:10.4171/cmh/71.

[25] Bruno Martelli and Carlo Petronio. Three-manifolds having complexity at most 9. *Experiment. Math.*, 10(2):207–236, 2001. doi:10.1080/10586458.2001.10504444.

[26] Sergei V. Matveev. *Algorithmic Topology and Classification of 3-Manifolds*, volume 9 of *Algorithms and Computation in Mathematics*. Springer-Verlag, second edition, 2007. doi:10.1007/978-3-540-45899-9.

[27] Sergei V. Matveev. Atlas of 3-Manifolds. <http://www.matlas.math.csu.ru/>, accessed November 2022.

[28] Grisha Perelman. The entropy formula for the Ricci flow and its geometric applications. [arXiv:math/0211159](https://arxiv.org/abs/math/0211159), 2002.

[29] Grisha Perelman. Finite extinction time for the solutions to the Ricci flow on certain three-manifolds. [arXiv:math/0307245](https://arxiv.org/abs/math/0307245), 2003.

[30] Grisha Perelman. Ricci flow with surgery on three-manifolds. [arXiv:math/0303109](https://arxiv.org/abs/math/0303109), 2003.

[31] Riccardo Piergallini. Standard moves for standard polyhedra and spines. In *III Convegno Nazionale Di Topologia: Trieste, 9-12 Giugno 1986 : Atti*, number 18 in *Rend. Circ. Mat. Palermo (2) Suppl.*, pages 391–414, 1988. doi:11581/244540.

[32] J. Hyam Rubinstein. An algorithm to recognize the 3-sphere. In *Proceedings of the International Congress of Mathematicians*, pages 601–611. Birkhäuser, 1995. doi:10.1007/978-3-0348-9078-6_54.

[33] J. Hyam Rubinstein, Henry Segerman, and Stephan Tillmann. Traversing three-manifold triangulations and spines. *Enseign. Math.*, 65(1/2):155–206, 2019. doi:10.4171/LEM/65-1/2-5.

[34] Francisco Santos. A counterexample to the Hirsch Conjecture. *Ann. of Math.*, 176(1):383–412, 2012. doi:10.4007/annals.2012.176.1.7.

- [35] Peter Scott. The geometries of 3-manifolds. *Bull. London Math. Soc.*, 15(5):401–487, 1983. doi:10.1112/blms/15.5.401.
- [36] Abigail Thompson. Thin position and the recognition problem for S^3 . *Math. Res. Lett.*, 1(5):613–630, 1994. doi:10.4310/MRL.1994.v1.n5.a9.
- [37] William P. Thurston. *Three-Dimensional Geometry and Topology*. Princeton University Press, 1997. doi:10.1515/9781400865321.
- [38] Jeff Weeks. Computation of hyperbolic structures in knot theory. In William Menasco and Morwen Thistlethwaite, editors, *Handbook of knot theory*, chapter 10, pages 461–480. Elsevier Science, 2005. doi:10.1016/B978-044451452-3/50011-3.

A More triangulations with no core edges

In section 5.1, we mentioned that in addition to finding a triangulation with no core edges for the 3-sphere, we also found such triangulations for the following lens spaces: $L_{6,1}$, $L_{9,2}$, $L_{11,2}$, $L_{13,3}$, and $L_{16,3}$. For these five additional cases, it was always enough to just run Algorithm 20 with $x = 0$ and 12 concurrent processes; the results are as follows:

- For $L_{6,1}$, we began with the isomorphism signature `dLQbcchhjs`. Figure 14 summarises the result of running Algorithm 20. We then used a breadth-first search to simplify down to a 12-tetrahedron example with isomorphism signature

`mLvwLLQQQadjljljgilkilkknaqlabamaqacv.`

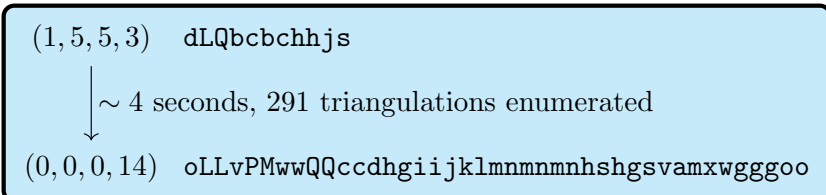


Figure 14: Removing core edges from `dLQbcchhjs` ($L_{6,1}$); $x = 0$, 12 processes.

- For $L_{9,2}$, we began with the isomorphism signature `dLQbcchhjw`. Figure 15 summarises the result of running Algorithm 20 twice. We then used a breadth-first search to simplify down to a 13-tetrahedron example with isomorphism signature

`nvLLMMAwQkcdghghjikml1mmmnkpmigoriulkkn.`

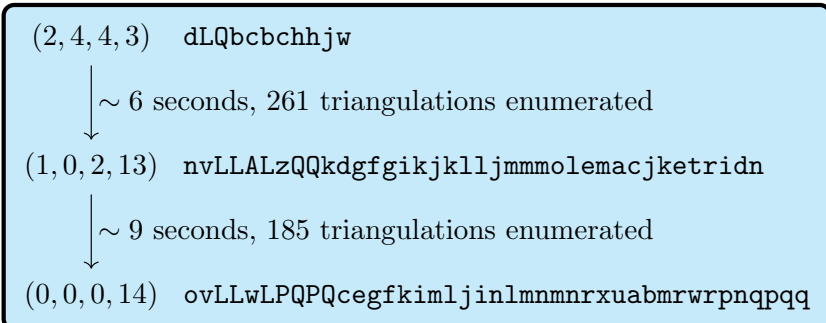


Figure 15: Removing core edges from `dLQbcchhjw` ($L_{9,2}$); $x = 0$, 12 processes.

- For $L_{11,2}$, we began with the isomorphism signature `eLAbcbddhhjhr`. Figure 16 summarises the result of running Algorithm 20 twice. We then used a breadth-first search to simplify down to a 16-tetrahedron example with isomorphism signature

`qLvwLPLvQQQkadhgkiknopknopponjajcxacsvvocvvvc.`

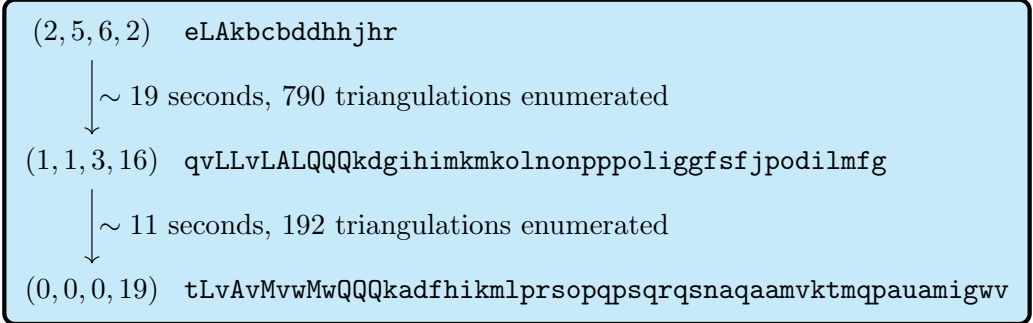


Figure 16: Removing core edges from `eLAbcbddhhjhr` ($L_{11,2}$); $x = 0, 12$ processes.

- For $L_{13,3}$, we began with the isomorphism signature `eLAbcbddhhjqn`. Figure 17 summarises the result of running Algorithm 20 twice. We then used a breadth-first search to simplify down to a 17-tetrahedron example with isomorphism signature

`rvLLALwwLQQQccdgfkhoqpqpononpqnkpisnsaaaanngngns.`

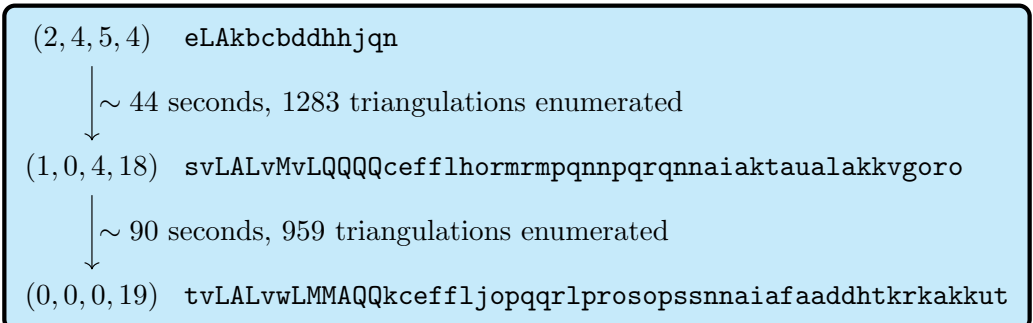


Figure 17: Removing core edges from `eLAbcbddhhjqn` ($L_{13,3}$); $x = 0, 12$ processes.

- For $L_{16,3}$, we began with the isomorphism signature `fLAMcbcbdeehhjhxj`. Figure 18 summarises the result of running Algorithm 20 twice. We then used a breadth-first search to simplify down to a 20-tetrahedron example with isomorphism signature

`uLvvvAvLzQPQQcadigooqmoslprtsprtstnaaoqovfctkfkfqlkfxta.`

B More triangulations with no tunnel edges

In section 5.2, we mentioned that we found triangulations with no tunnel edges for all but one of the prime knots with crossing number up to 7, but did not give detailed results for the cases with crossing number 6 and 7. We present these results here:

- For the 6_1 knot, we began with the isomorphism signature `gLLMQcceffdfeqldg`. Figure 19 summarises the results of running Algorithm 20 four times.

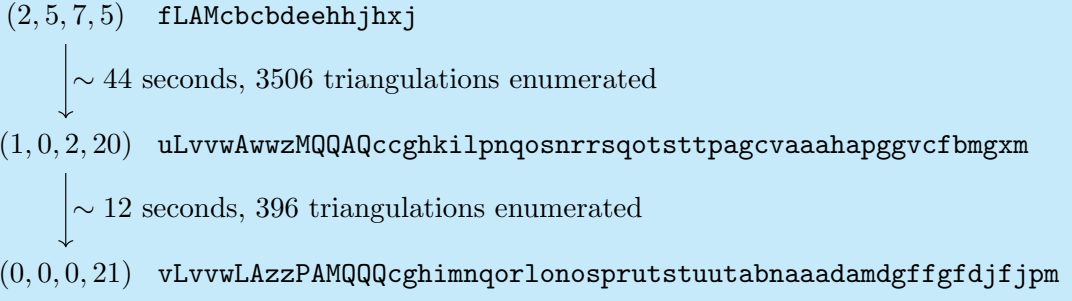


Figure 18: Removing core edges from $fLAMc...j$ ($L_{16,3}$); $x = 0, 12$ processes.

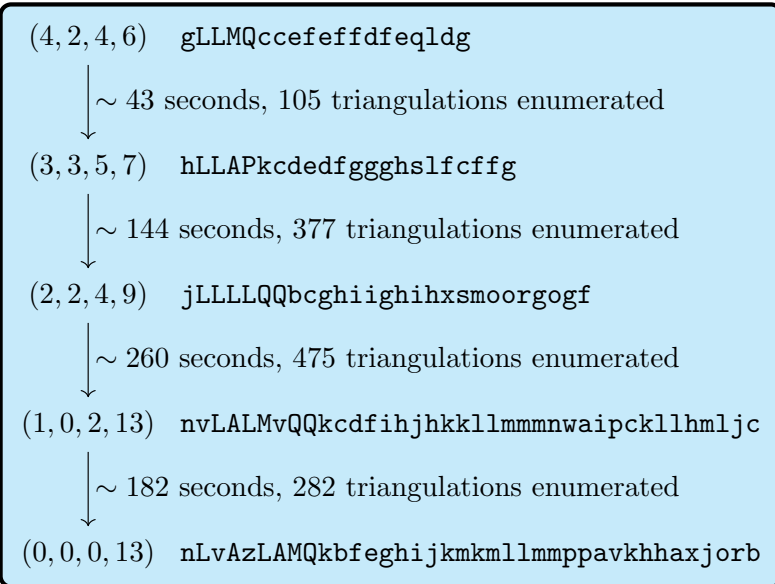


Figure 19: Removing tunnel edges from $gLLM...g$ (6_1 knot); $x = 0, 12$ processes.

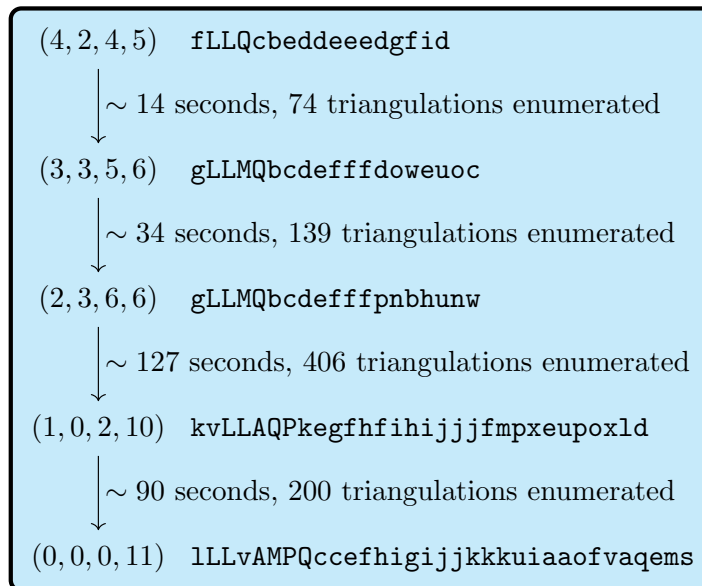


Figure 20: Removing tunnel edges from $fLLQ...d$ (6_2 knot); $x = 0, 12$ processes.

- For the 6_2 knot, we began with the isomorphism signature `fLLQcbbeddeedgfid`. Figure 20 summarises the results of running Algorithm 20 four times.
- For the 6_3 knot, we began with the isomorphism signature `eLPkbcdddcwjb`. Figure 21 summarises the results of running Algorithm 20 three times.

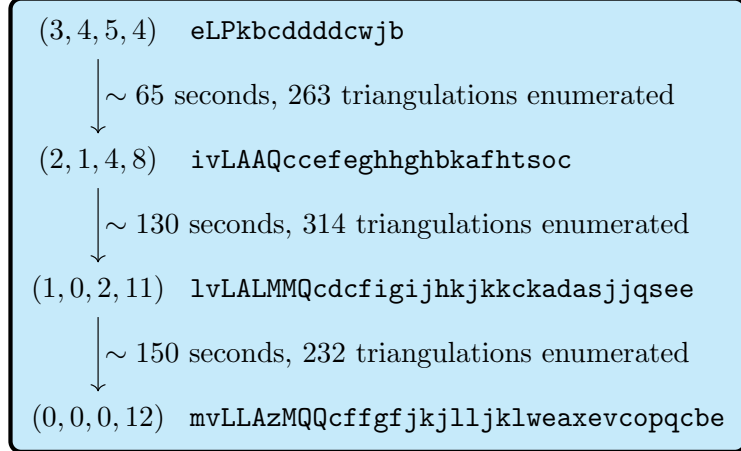


Figure 21: Removing tunnel edges from `eLPkbcdddcwjb` (6_3 knot); $x = 0, 12$ processes.

- For the $(7, 2)$ torus knot (also known as the 7_1 knot), we began with the isomorphism signature `eLAkbccddaeakln`. Figure 22 summarises the results of running Algorithm 20 twice.

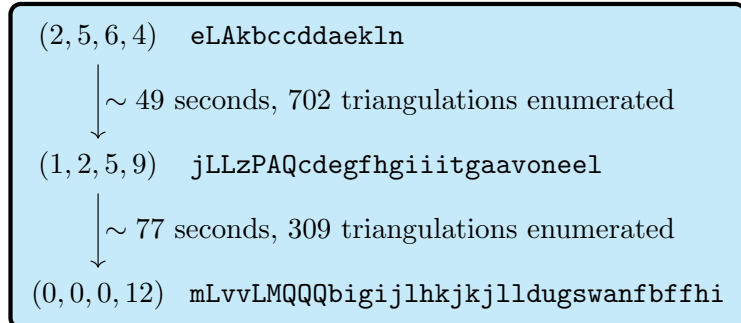


Figure 22: Removing tunnel edges from `eLAkbccddaeakln` ((7, 2) torus knot); $x = 0, 12$ processes.

- For the 7_2 knot, we began with the isomorphism signature `eLAkbccddmejln`. Figure 23 summarises the results of running Algorithm 20 three times.
- For the 7_3 knot, we began with the isomorphism signature `fLLQcbbeddeedgfa`. Figure 24 summarises the results of running Algorithm 20 four times.
- For the 7_4 knot, we began with the isomorphism signature `gLLAQbdedffffdwmfarv`, which has complexity $(4, 2, 4, 6)$. To reduce the number of tunnel edges to 3, we needed to run Algorithm 20 with 24 concurrent processes (12 processes was not enough). After that, it was enough to run Algorithm 20 three times with 12 concurrent processes. The results are summarised in Figure 25.
- For the 7_5 knot, we began with the isomorphism signature `hLLAMkbedefgggtlftavkb`. Figure 26 summarises the results of running Algorithm 20 five times.
- For the 7_6 knot, we began with the isomorphism signature `iLLvQQccdeggfhhhdoldgrgnk`. Figure 27 summarises the results of running Algorithm 20 four times.
- For the 7_7 knot, we began with the isomorphism signature `iLLPzQcbcffghghhmomtdirhx`, which has complexity $(4, 2, 4, 8)$. To reduce the number of tunnel edges to 3, we needed to run Algorithm 20 with 24 concurrent processes (12 processes was not enough). After that, it was enough to run Algorithm 20 three times with 12 concurrent processes. The results are summarised in Figure 28.

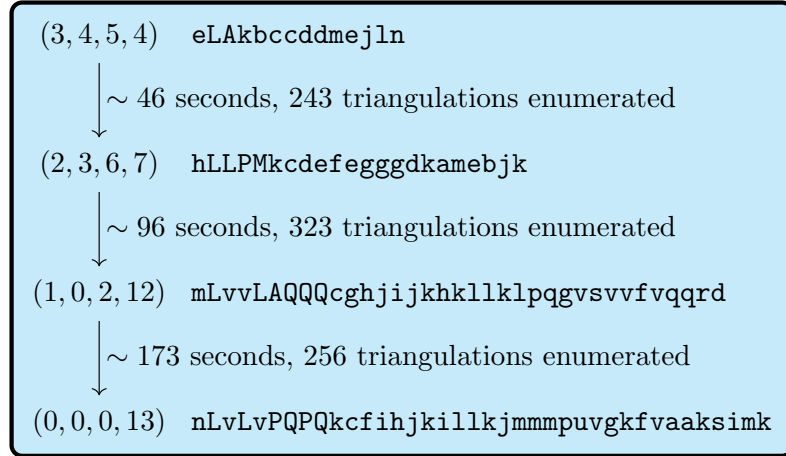


Figure 23: Removing tunnel edges from `eLAkbccddmejln` (7₂ knot); $x = 0, 12$ processes.

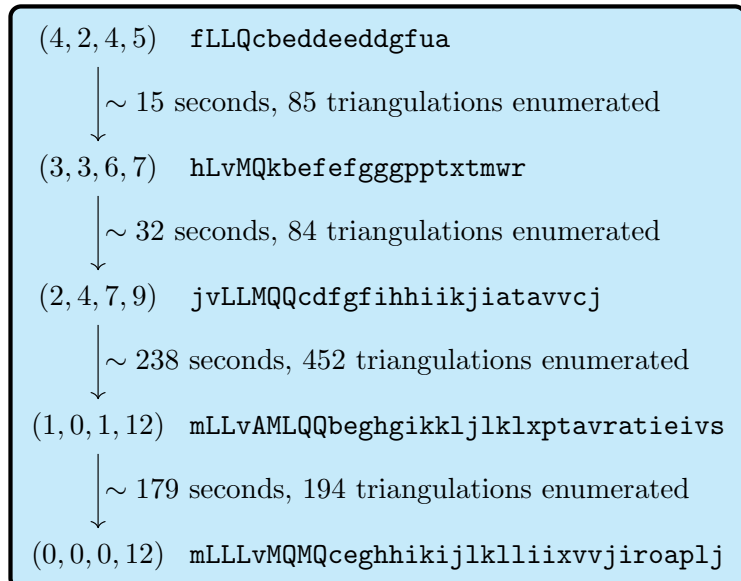


Figure 24: Removing tunnel edges from `fLLQcbeddeeddgfua` (7₃ knot); $x = 0, 12$ processes.

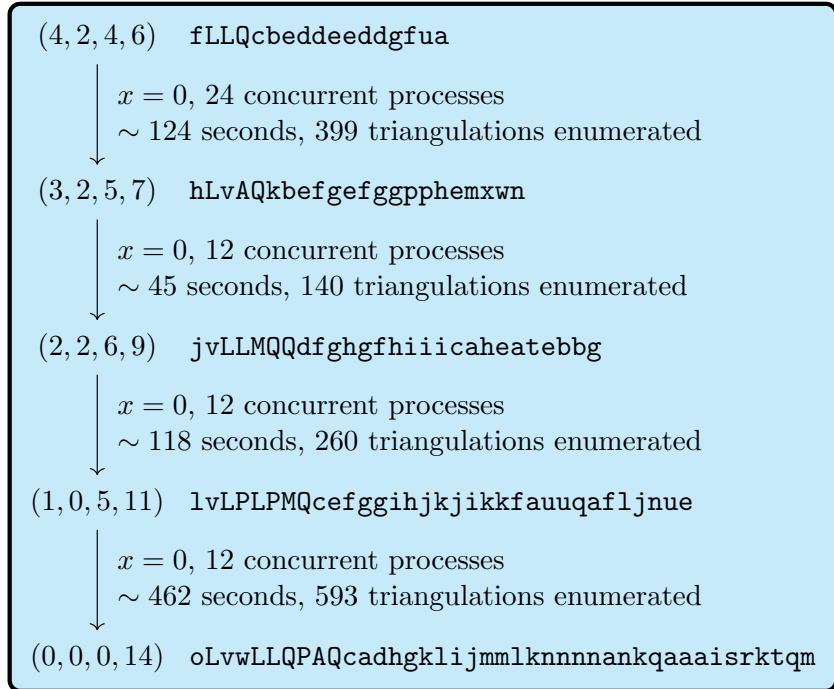


Figure 25: Removing tunnel edges from $gLLAQbdedffffdwmfarv$ (7₄ knot).

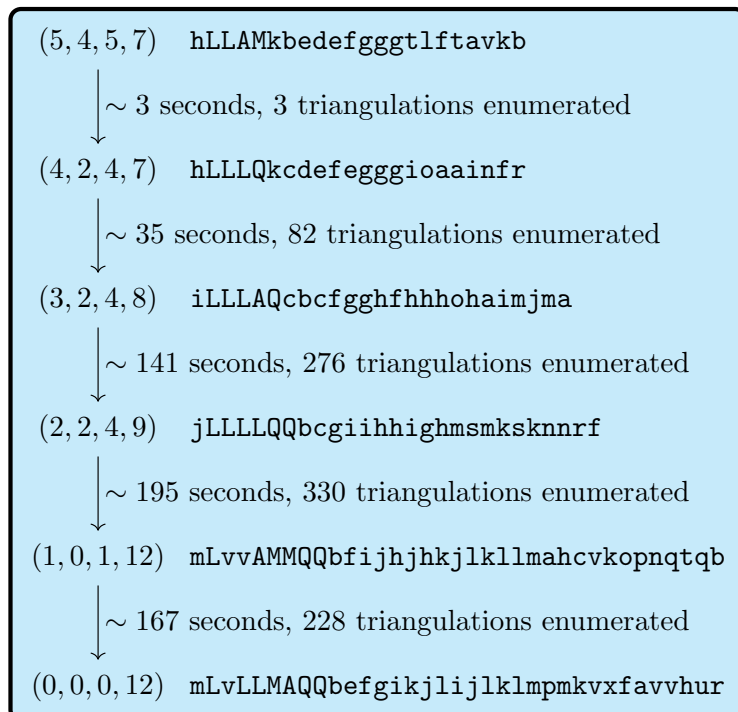


Figure 26: Removing tunnel edges from $hLLAMkbedefgggtlftavkb$ (7₅ knot); $x = 0$, 12 processes.

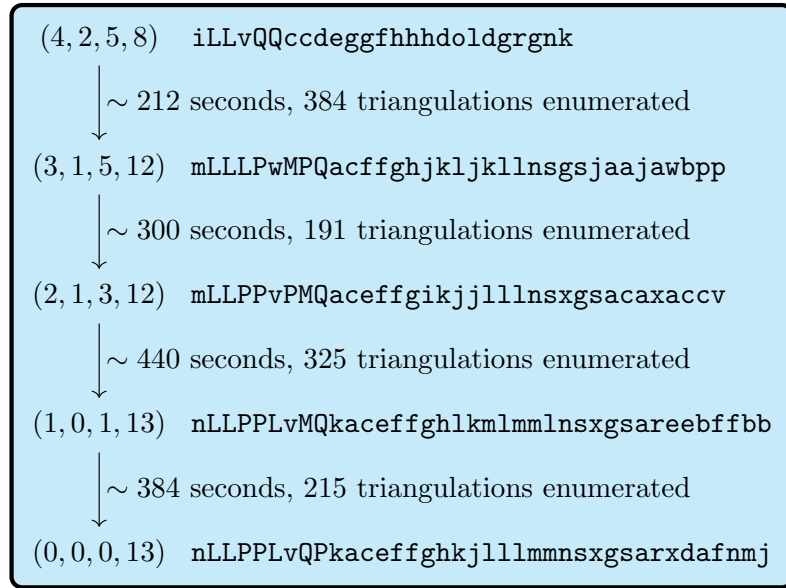


Figure 27: Removing tunnel edges from $iLLvQQccdeggfhhh\cancel{old}grgnk$ (7₆ knot); $x = 0, 12$ processes.

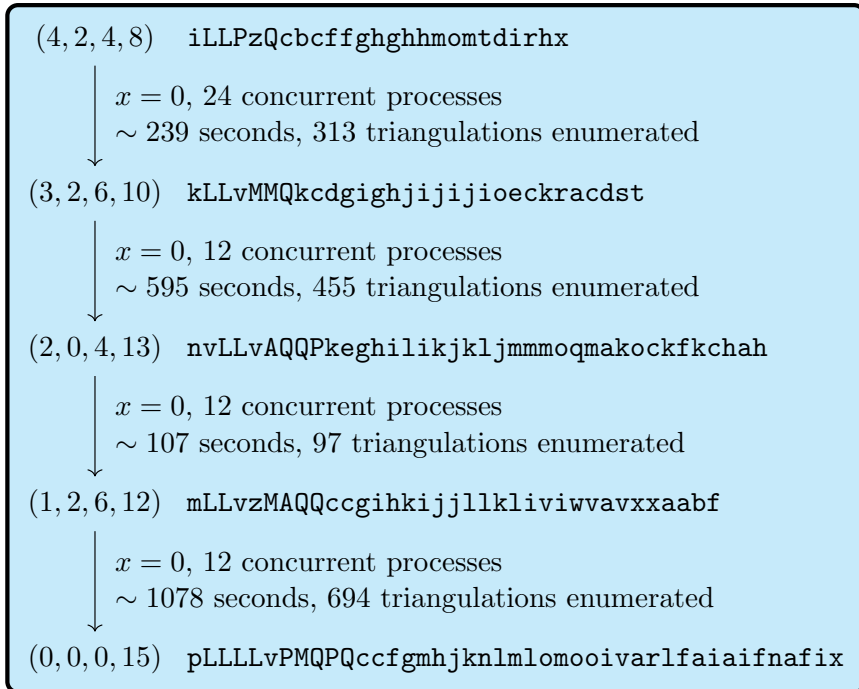


Figure 28: Removing tunnel edges from $iLLPzQcbc~~ff~~ghgh\cancel{hm}omtdirhx$ (7₇ knot).